Enhancer priming enables fast and sustained transcriptional responses to Notch signaling.

Julia Falo-Sanjuan[1], Nicholas C Lammers[2], Hernan G Garcia[2,3,4,5], Sarah Bray[1]*,

1 Department of Physiology, Development and Neuroscience. University of Cambridge, UK

2 Biophysics Graduate Group, University of California at Berkeley, Berkeley, California

3 Department of Physics, University of California at Berkeley, Berkeley, California

4 Department of Molecular and Cell Biology, University of California at Berkeley, Berkeley, California

5 Institute for Quantitative Biosciences-QB3, University of California at Berkeley, Berkeley, California

*** Correspondence**

Abstract

Information from developmental signaling pathways must be accurately decoded to generate transcriptional outcomes. In the case of Notch, the intracellular domain (NICD) transduces the signal directly to the nucleus. How enhancers decipher NICD in the real time of developmental decisions is not known. Using the MS2/MCP system to visualize nascent transcripts in single cells in *Drosophila* embryos we reveal how two target enhancers read Notch activity to produce synchronized and sustained profiles of transcription. By manipulating the levels of NICD and altering specific motifs within the enhancers we uncover two key principles. First, increased NICD levels alter transcription by increasing duration rather than frequency of transcriptional bursts. Second, priming of enhancers by tissue-specific transcription factors is required for NICD to confer synchronized and sustained activity; in their absence, transcription is stochastic and bursty. The dynamic response of an individual enhancer to NICD thus differs depending on the cellular context.

Introduction

Genes respond to external and internal cues through the action in the nucleus of transcription factors and effectors of signalling pathways. Regulatory regions that surround genes, termed enhancers, integrate the information from these inputs to produce an appropriate transcriptional output. During development some of these decisions can occur in a matter of minutes, but usually the outcomes are measured many hours later. Rarely have transcription dynamics been analyzed *in vivo* in the real-time of the developmental signalling pathways, so we know little about how recipient enhancers decipher the signals. For example, enhancers could respond in a digital manner, working as simple on off switches, or as analog devices, operating as a rheostat so that levels of the signal can modulate the output (Blackwood et al. 1998; Garcia et al. 2013; Lammers et al. 2018). In either case they must also have the capability to detect and transduce key parameters to the transcription machinery, such as input signal duration and thresholds.

With the advent of precise and quantitative methods to measure transcription, such as single molecule fluorescence in situ hybridization (smFISH) or live imaging, it has become evident that transcription is not a continuous process. Instead, genes that are being actively transcribed undergo bursts of initiation that are often separated by inactive intervals (Chubb et al. 2006; Golding et al. 2005). Bursting is thought to occur because the dynamics of enhancer-promoter activation leads to episodic polymerase release. One consequence of this behaviour is that factors modulating the output levels of transcription can do so by changing either the frequency with which a burst occurs (measured by the gap between bursts) or the size of each burst (measured by changes in burst duration and/or amplitude). Since forced looping of the *beta-globin* enhancer to its promoter led to an increase in burst frequency (Bartman et al. 2016), it has been proposed that transcription factors activate transcription by modulating enhancer-promoter interactions, and hence bursting frequency; although other studies suggest enhancer-promoter interactions are not the underlying basis of transcriptional bursting (Lim et al. 2018; Chen et al. 2018). Though the molecular origin of bursting remains unknown, bursting frequency rather than burst duration or amplitudes seems to be the major parameter modulated in different species and contexts (So et al. 2011; Senecal et al. 2014; Xu et al. 2015; Desponds et al. 2016; Padovan-Merhar et al. 2015; Lammers et al. 2018; Berrocal et al. 2018). For example, enhancers controlling early patterning genes in *Drosophila* embryos all produce similar bursting size but have different bursting frequencies, which can be attenuated by the presence of insulators (Fukaya et al. 2016). Similarly, steroids increase the bursting frequency of target enhancers to regulate their activation kinetics (Larson et al. 2013; Fritzsch et al. 2018). However, it remains to be discovered whether all transcription factors alter transcription dynamics in this way and specifically whether it is these or other properties that are

modulated by developmental signals to confer appropriate outputs in the *in vivo* setting of a developing organism.

Transcriptional bursting is thought to make an important contribution to heterogeneity in the output of transcriptional activity between cells (Raj et al. 2008). For example, in cells exposed to estrogen, response times for activation of transcription measured live were highly variable and there was no coherent cycling between active and inactive states (Fritzsch et al. 2018). Stochastic transcriptional behaviour has been found of key importance in many developmental decisions, such as the differentiation of photoreceptors in the *Drosophila* eye (Wernet et al. 2006), hematopoietic cell differentiation in mouse cells (Chang et al. 2008; Ng et al. 2018) or during neuronal differentiation in the zebrafish retina (Boije et al. 2015). But while an attractive feature for promoting heterogeneity, inherent variability in responses could be extremely disruptive in developmental processes where the coordinated response of many cells is required to pattern specific structures. In some cases this may be circumvented by mechanisms that allow cells to achieve the same average mRNA output and so produce homogeneous patterns of gene expression (Little et al. 2013). For example, cells that express the mesodermal determinant Snail average their transcriptional output over a period of 20 minutes by mRNA diffusion to produce a homogeneous field of cells and a sharp boundary in *Drosophila* syncytial embryos (Bothma et al. 2018). However it is only in rare circumstances that mRNA diffusion can operate and it is unclear whether other averaging mechanisms would be effective over shorter time intervals. To effectively achieve reproducible patterns, cells must therefore overcome the variability that is inherent in transcriptional bursting and stochastic enhancer activation.

Notch signaling is one highly conserved developmental signaling pathway that is deployed in multiple different contexts. It has the unusual feature that the Notch intracellular domain (NICD) transduces the signal directly to the nucleus, when it is released by a series of proteolytic cleavages precipitated by interactions with the ligands. NICD then stimulates transcription by forming a complex with the DNA binding protein CSL and the co-activator Mastermind (Mam) (Bray 2006). The lack of intermediate signalling steps and amplification makes this a powerful system to investigate how signals are deciphered by responding enhancers. Furthermore, there may be differences in the levels and dynamics of NICD produced by different ligands (Nandagopal et al. 2018). However, although its role as a transcriptional activator is well established, at present we know little about how enhancers respond to NICD in the real time of developmental decisions. For example, do the enhancers operate as simple switches, detecting when NICD crosses a threshold? Or are they sensitive to different levels of NICD, in which case does NICD, like other factors, modulate bursting frequency? Nor do we know what features in the sequence of the responding enhancers confer the output properties, although it has been suggested that enhancers with paired CSL motifs (referred to as SPS motifs)(Bailey et al. 1995; Nam et al. 2007), whose precise spacing could favour NICD-NICD dimerization, have the potential to yield the strongest responses (Nam et al. 2007).

In order to determine how enhancers respond to Notch activity in real time we have used the MS2/MCP system to visualize nascent transcripts in *Drosophila* embryos. To do so we used two well-characterised Notch responsive enhancers that drive expression in a stripe of mesectoderm (MSE) cells and analyzed the levels of transcription they produced over time at the single cell level. Strikingly all MSE cells initiate transcription within a few minutes of one another, and once active, each nucleus produced a sustained profile of transcription, without distinct bursts. By manipulating the levels of NICD and altering key motifs within the enhancers we uncover two key principles. First, the ability of NICD to confer synchronized and sustained activity in MSE requires that the enhancers are primed by tissue-specific transcription factors. In their absence, MSE enhancers confer stochastic bursty transcription profiles, demonstrating that different response profiles can be generated from a single enhancer according to which other factors are present. Second, changing Notch levels modulates the transcription burst size but not length of the periods between bursts, in contrast to most current examples for enhancer activation. These two key concepts, that we have uncovered by analysing the dynamics of transcription profiles produced by enhancer variants in different signalling conditions, are likely to be of general importance for gene regulation by other signalling pathways in developmental and disease contexts.

Results

Synchronised and sustained enhancer activation in response to Notch

To investigate how Notch signals are read out in real time, we focused on the well-characterized mesectodermal enhancers (MSEs) from the *Enhancer of split-Complex (E(spl)-C)* (known as *m5/m8*) and from *singleminded* (*sim*) (Morel et al. 2000; Cowden et al. 2002; Zinzen et al. 2006a). These direct expression in two stripes of MSE cells when Notch is activated in response to Delta signals from the presumptive mesoderm (Fig. 1**AB**) (Morel et al. 2003; De Renzis et al. 2006; Zinzen et al. 2006a). The MSE converge to the midline during gastrulation, ultimately forming CNS midline precursors similar to the vertebrate floorplate. To visualize transcription from these enhancers in real time, they were inserted into MS2 reporter constructs containing the promoter from the gene *even-skipped* (*peve*), 24 *MS2* loops and the *lacZ* transcript (Fig. 1**A**). When these *MS2* reporters were combined with MCP-GFP in the same embryos, nascent transcription was marked by the accumulation of MCP-GFP in bright nuclear puncta, where the total fluorescence in each spot is directly proportional to the number of transcribing mRNAs at any timepoint (Fig. 1**AB**)(Garcia et al. 2013). In this way the levels of transcription can be followed over time at the single cell level by tracking the puncta relative to the nuclei (which were labelled with His2Av-RFP).

By visualizing transcription in real time, we could see that both *m5/m8* and *sim* switched on transcription

in all cells along the MSE stripe within a narrow time-window (~ 10 min) in nc14 (Fig. 1**CDE**). We note that both enhancers also directed earlier, Notch independent transcription, in broad domains in nuclear cycles 10 to 13 (**Movie 1. Movie 2.**) and in the first few minutes of nuclear cycle 14 in few scattered cells. However, this was followed by a long period (approximately 20 min) of inactivity before the cells in the MSE stripe initiated transcription concurrently. *m5/m8* and *sim* were then active in a sustained manner in all nuclei - few separated bursts of transcription were detected - throughout the remaining period of nc14 as the embryos underwent the first stage of gastrulation (mesoderm invagination) (Fig. S1**E**). Transcription then ceased after 30-50 minutes, with less synchrony than at the onset (Fig. 1**E**).

Sustained activity is a feature of *m5/m8* and *sim* and not a general property of Notch responsive enhancers, as a neuroectodermal enhancer from *E(spl)m8-bHLH* (*m8NE*, Fig. 1**A**) exhibited delayed and stochastic activity in the MSE at this stage (Fig. S1**AB**). Furthermore, even though the profiles produced by *m5/m8* and *sim* were continuous, the amplitude fluctuated, likely reflecting episodic polymerase release. However it is notable that *m5/m8* and *sim* both direct transcription profiles that are highly co-ordinated temporally, with each conferring a prolonged period of activity that is initiated within a short time-window. Indeed, the mean profile of all the MSE cells was almost identical for the two enhancers (Fig. 1**F**). This is remarkable given that they contain different configurations of binding motifs and implies that the mesectoderm cells undergo a highly synchronized period and level of Notch signaling.

We next tested the consequences from substituting different promoters with the *m5/m8* and *sim* enhancers, to assess the relative contributions of the enhancer and promoter to the response profiles. First, when *peve* was replaced by a promoter from *sim* (*psimE*), both *m5/m8* and *sim* produced lower levels of transcription, but their overall temporal profiles remained similar and the mean levels were the same for the two enhancers (Fig. S1**C**). Second, we combined *m5/m8* with another heterologous promoter, *hsp70*, and with four promoters from the *E(spl)-C* genes that could be interacting with *m5/m8* in the endogenous locus. Similar to *psimE*, substituting these promoters also led to changes in the mean levels of transcription without affecting the overall temporal profile or expression pattern (Fig. S1**D**). Notably, even in combinations where the overall levels were lower, the transcription profiles remained sustained rather than breaking down into discrete bursts (Fig. S1**E**) consistent with promoters affecting mean levels of activity without modulating bursting frequencies. Of those tested, *pm6* produced the lowest mean levels when combined with *m5/m8* (Fig. S1**D**). This is consistent with the fact that *E(spl)m6-BFM* is not normally expressed in the MSE and argues for an underlying enhancer-promoter compatibility at the sequence level (Fig. S1**D**)(Zabidi et al. 2014). Nevertheless, the fact that similar temporal profiles were produced with all the promoters confirms that the enhancers are the primary detectors of Notch signaling activity.

To verify that nc14 MSE transcription was indeed Notch-dependent we measured transcription from *m5/m8* in embryos where Notch activity was disrupted by mutations. Embryos lacking Neuralized, an E3 ubiquitin ligase required for Delta endocytosis that is critical for Notch signalling (Morel et al. 2003; De Renzis et al. 2006), had no detectable transcription from *m5/m8* in the MSE (Fig. 1**G**). Likewise, *m5/m8* activity was severely compromised in embryos carrying mutations in *Delta*. Because Delta protein is deposited in the egg maternally (Kopczynski et al. 1988), these embryos contained some residual Delta which was sufficient for a few scattered cells in the MSE stripe to initiate transcription (Fig. S1**F**). However their transcription ceased prematurely, within <20 min (Fig. 1**G**, S1**F**). Together these results confirm that the enhancers require Notch signalling for their activity in the MSE, in agreement with previous studies of these regulatory regions (Morel et al. 2000; Zinzen et al. 2006a), and further show that sustained Notch signalling is needed to maintain transcription, arguing that the enhancers are also detecting persistence of NICD.

Coordinated activity of enhancers within each nucleus

Although *m5/m8* and *sim* confer well coordinated temporal profiles of transcriptional activity, there is nevertheless some cell to cell variability in the precise time of their activation. To investigate whether this cell to cell variability was due to the stochastic nature of transcription (intrinsic variability) or whether it indeed reflects changes in signalling from Notch (extrinsic variability) (Elowitz 2002; Raser et al. 2006) we monitored expression from two identical alleles of the MS2 reporters, supplied by the paternal and maternal chromosomes (Fig. 2**A**). Transcription from these two physically unlinked loci were detected as distinct puncta in each nucleus so that each one could be tracked independently. We found a remarkable synchrony in the onset of transcription from both alleles of a given enhancer (Fig. 2**B**). More than 80% of the cells initiated transcription from both alleles less than 5 min apart, (Fig. S2**C**), which contributes to $\sim$ 6-30% of the total variability (Fig. 2**D**), indicating that most of the temporal variability in transcription onset between cells was due to extrinsic factors. There was less synchrony between the two alleles in the time at which transcription was extinguished (Fig. 2**B** S2**A**), but the extent of variability was much lower than that between cells (only contributing to less than 15% of the total variability, Fig. 2**D**) and it likely occurs because there will be locus to locus variations in the stage of the transcriptional bursting cycle when the signaling levels decline

Although the overall temporal profiles of transcription from the two alleles were similar to one another, in terms of the onset and overall increases or decreases in levels, the fine grained spikes and troughs were not synchronised (Fig. 2**A**), in agreement with the expectation that transcription from two different loci is largely uncorrelated (Harper et al. 2011; Little et al. 2013; Fritzsch et al. 2018). However, the fluorescent intensities of

two alleles at any time point displayed a small but significant positive correlation ($R^2 \sim 0.35$), compared to a null correlation when these pairs are randomly assigned (Fig. S2**B**). This argues that the enhancers at the two alleles operate independently while being co-ordinated by the same extrinsic signal information, namely the durations and levels of Notch activity. Even when the *m5/m8* and *sim* enhancers were placed in trans in the same cell, there was comparatively little variation in the onset times, compared to the variation in the onset of the enhancers in different cells (Fig. 2**CD** S2**A**). These results indicate that *m5/m8* and *sim* are reliably detecting extrinsic information in the form of Notch activity, which is initiated in the mesectoderm cells within a 5-10 minute time-window, so that within a given nucleus their activation is remarkably synchronized.

Enhancers detect signal thresholds and signal context

The *m5/m8* and *sim* enhancers appear to act as "persistence detectors", driving transcription as long as Notch signal(s) are present. They may therefore be simple switches detecting when a signal crosses a threshold (digital encoding). Alternatively, the enhancers could respond in a dose-sensitive manner to the levels of Notch activity (analog encoding). To distinguish these possibilities, we tested the consequences from additional Notch activity, by supplying ectopic NICD using the *stripe 2* regulatory enhancer from the *even-skipped* gene (*eve2-NICD*). This confers a tightly regulated ectopic stripe of NICD which is orthogonal to the MSE (Fig. 3**A**) (Kosman et al. 1997; Cowden et al. 2002) and was sufficient to produce ectopic expression from both *m5/m8* and *sim* driven reporters (**Movie 3.Movie 4.**).

Whereas expression from *m5/m8* and *sim* was almost identical in wild-type embryos, clear differences in their behaviour were revealed by ectopic NICD. First, transcription from *m5/m8* was detected throughout much of the region corresponding to the *eve2* stripe whereas ectopic transcription from *sim* was only seen in 3-4 cell wide region dorsal to the MSE (Fig. 3**B**), consistent with previous observations (Cowden et al. 2002; Zinzen et al. 2006a). Second, although both enhancers initiated transcription prematurely, because the ectopic NICD was produced from early nc14 (Bothma et al. 2014), the onset of transcription from *m5/m8* was significantly earlier than that from *sim* (Fig. 3**DE**). Given that both enhancers are exposed to the same temporal pattern of NICD production, this difference in their initiation times implies that the two enhancers have different thresholds of response to NICD, with *m5/m8* responding to lower doses and hence being switched-on earlier. Therefore, we hypothesize that *m5/m8* and *sim* respond at the same time in wild-type embryos because the normal ligand-induced signaling leads to a sharp increase in NICD.

We also detected differences in the dynamics of *m5/m8* according to the location of the NICD-expressing

nucleus along the DV axis. Nuclei closer to the MSE stripe (in the neuroectoderm, NE) exhibited strong activity, with a temporal pattern that resembled that in the MSE (Fig. 3**C**, bottom). In contrast nuclei in dorsal regions (dorsal ectoderm, DE) underwent resolved bursts of transcriptional activity (Fig. 3**C**, top). Ectopic NICD also induced 'bursty' expression from *sim* in the mesoderm (ME), but was not capable of turning on *m5/m8* in that region (**Movie 5.**). The positional differences in dynamics suggest that intrinsic cellular conditions, likely the expression levels of specific transcription factors, influence the way that enhancers "read" the presence of NICD. Such factors must therefore have the capability to modulate the dynamics of transcription.

The fact that *m5/m8* and *sim* are switched on at different times in the presence of ectopic NICD suggests that they require different thresholds for their activation. In addition, they only give sustained transcription profiles in a 2-3 cell-wide region overlapping the MSE, whereas elsewhere they generate stochastic and "bursty" transcription, arguing that they must be differently primed in the MSE region.

Notch activity tunes transcription burst size

To further test how Notch responsive enhancers respond to different doses of signal, we introduced a second *eve2-NICD* transgene. MSE transcription from *sim* in the presence of 2x*eve2-NICD* initiated earlier and achieved higher levels than with 1x*eve2-NICD* (Fig. 4**A**, left). This is consistent with the hypothesis that the *sim* enhancer responds to thresholds of NICD concentration, as the cells will reach a given concentration of signal more quickly in the embryos with 2x*eve2-NICD*. The mean levels of transcription increased in the ME as well as in the MSE regions (Fig. 4**A**-**C**), further indicating a dose-sensitive response. In contrast, the levels and onset of MSE transcription from *m5/m8* did not significantly change in 2x*eve2-NICD* embryos (Fig. 4**A**, right). The output levels of transcription from the *m5/m8* enhancer therefore reached a saturation point with the dose produced by 1x*eve2-NICD*, possibly due to limiting levels of other factors at this stage. This only occurred in the MSE, as the more stochastic activity in the DE remained sensitive to increases in NICD, becoming responsive in a greater proportion of cells and remaining active over longer periods (Fig. S4**A**).

To distinguish different models for how NICD confers a dose-sensitive response, we took two strategies to analyze its effect on the transcriptional bursting dynamics. Both approaches assume a two state model where the promoter is switched between an OFF and ON state with switching rates *Kon* and *Koff* (representative of the probabilities of switching the enhancer on and off respectively) and confers transcription initiation rate r in the ON state (Fig. 4**E**)(Peccoud et al. 1995; Larson et al. 2009). In the first approach we used the parameters of bursting amplitude, off period between bursts and bursting length as approximations for r, *Kon* and *Koff*, respectively (Fig.

4**E**). In most previous enhancers analyzed in this way, the off period is the most affected, leading to changes in the frequency of bursting (Fukaya et al. 2016; Fritzsch et al. 2018; Lammers et al. 2018). However, when we quantified the effect from different doses of NICD on *sim* in the ME, a region where individual bursts of transcription could be distinguished, we found that the bursting length consistently increased with higher amounts of NICD whereas the off period between bursts remained constant (Fig. 4**DF**). This indicates that the main effect of NICD is to keep the enhancer in the ON state for longer - ie. decreasing *Koff* - rather than increasing the frequency with which it becomes active (i.e. increasing *Kon*). The bursting amplitude also increased with 1x*eve2-NICD* but this was not further enhanced by 2x*eve2-NICD* (Fig. 4**DF**). Overall therefore, increasing levels of NICD in the ME result in *sim* producing an increase in transcription burst size (duration x amplitude) rather than an increase in the frequency of bursts. Transcription in other regions and enhancers (*m5/m8* DE and *m8NE* ME) showed similar increase in burst size in response to the dose of NICD (Fig. S4**A**-**C**) suggesting this is a general property of these Notch responsive enhancers.

We developed a second approach, based on the noise properties of transcription, to analyze the changes in the dynamics where single bursts of activity could not be defined. To do so, we used a mathematical model of transcription to account for the initiating mRNA molecules (Fig. S3**A**). Using derivations from the mathematical model and testing them in simulations, we looked for the signatures that would be produced if the mean of initiating mRNAs (equivalent to the mean fluorescence from the MS2 puncta) were increasing due to changes in r, *Kon* or *Koff*. This showed that the effects on the Fano factor ratio between the two conditions and on their autocorrelation function (ACF) could be used to correctly predict which of the three parameters could account for the increase in the mean (Fig. S3**B**, Supplementary Methods). First we tested the modelling approach with the data from the promoter swap experiments. Analyzing the differences in the mean indicated that they are most likely due to increases in r (Fig. S4**D**), as expected if promoters influence the rate of polymerase release but not the activation of the enhancer per se. When we then applied the model to the data from the transcription profiles produced by different doses of NICD in the ME the results were most compatible with the causal effect being a increase in r or a decrease in *Koff* (Fig. S4**E**) depending on which two conditions were compared, i.e. this approach also indicated that NICD elicits an increase in burst size rather than in burst frequency. Thus the two approaches both converged on the model that, above the critical threshold level of NICD, further increases in NICD levels prolong the period that each enhancer remains in the ON state.

Finally, we then used an enhancer - promoter combination that produces higher mean levels (*m5/m8-pm5*, Fig. S1**D**) to investigate whether the saturation that occurred with ectopic NICD was due to the *peve* promoter having achieved a maximal initiation rate. Strikingly, the substitution of *pm5* did not result in significantly higher

maximal levels than *m5/m8-peve* in the presence of *eve2-NICD* (Fig. S4**F**) although it did in wild-type signaling conditions (Fig. S1**D**). This result indicates that the saturation of the *m5/m8* response that occurs with higher levels of NICD stems from the *m5/m8* enhancer rather than the promoter and argues that enhancers reach a maximal "ON" state that they cannot exceed even if more NICD is provided.

Paired CSL motifs augment burst-size not threshold detection

The *m5/m8* and *sim* enhancers both respond to NICD but they initiate transcription at different thresholds. How is this encoded in their DNA sequence? A prominent difference between the two enhancers is that *m5/m8* contains a paired CSL motif (so-called SPS motifs), a specific arrangement and spacing of binding motifs that permit dimerization between complexes containing NICD (Nam et al. 2007), whereas *sim* does not (Fig, S5**A**). To test their role, we replaced two of the CSL motifs in *sim* with the SPS motif from *m5/m8* and conversely perturbed the SPS in *m5/m8* by increasing the spacing between the two CSL motifs (Fig. S5**A**). As SPS motifs permit co-operative binding between two NICD complexes, we expected that enhancers containing an SPS motif (sim^{SPS} and *m5/m8*) would exhibit earlier onsets of activity than their cognates without (*sim* and $m5/m8^{insSPS}$). However this was not the case for either *sim* and sim^{SPS} (Fig. 5**AB**) or *m5/m8* and $m5/m8^{insSPS}$ in either wild type or *eve2-NICD* embryos (Fig. S5**DE**). These profiles suggest that the SPS motifs are not responsible for the difference in the threshold levels of NICD required for *m5/m8* and *sim* activation.

Changes to the CSL motifs did however affect the mean levels of activity. sim^{SPS} directed higher mean levels of activity compared to *sim* in both wild type and *eve-NICD* embryos (Fig. 5**A** S5**B**). Conversely, $m5/m8^{insSPS}$ directed lower levels compared to *m5/m8* (Fig. S5**D**). Analysing the traces from *sim* enhancer in the ME, where cells undergo bursts of transcription, revealed that the SPS site (sim^{SPS}) led to larger burst-sizes - i.e. increased the amplitude and the duration - compared to the wild type enhancer without SPS sites (*sim*) (Fig. 5**CD**). Conversely, the continuous profile produced by *m5/m8* in the MSE was broken into smaller bursts when the SPS was disrupted (Fig. S5**FG**). The effects on the bursting size are similar to those seen when the dose of NICD was altered, suggesting that enhancers containing SPS sites respond to a given level of NICD more effectively. They do not however appear to affect the amount of NICD required for their initial activation, i.e. the threshold required for the enhancer to be switched on. This implies that the burst-size modulation and response threshold can be uncoupled and potentially could be encoded independently at the DNA level.

Regional factors prime enhancers for fast and sustained activation

Under ectopic NICD conditions, *m5/m8* and *sim* both produce sustained transcription profiles in the region overlapping the MSE and NE, whereas elsewhere they generate stochastic and "bursty" transcription. This suggests that other factors are "priming" the enhancers to respond to NICD. Good candidates are the factors involved in DV patterning at this stage, the bHLH transcription factor Twist (Twi) and/or the Rel protein Dorsal (dl). Indeed, the region where the enhancers generate sustained profiles in response to *eve2-NICD* coincides with the domain of endogenous Twist and Dorsal gradients (Fig S6**B**)(Zinzen et al. 2006b). Furthermore, *m5/m8* and *sim* both contain Twist and Dorsal binding motifs (Fig. S6**A**) and previous studies indicated that Twist is important for activity of *sim* although it was not thought to contribute to the activity of *m5/m8* (Zinzen et al. 2006a).

To test if Twist and Dorsal are responsible for the different dynamics of transcription observed in *m5/m8* we mutated Twist and/or Dorsal binding motifs in *m5/m8*, which normally exhibits strong activity in the MSE and NE and a 'bursty' pattern in DE cells in conditions of ectopic Notch activity (Fig. 3**B**). Strikingly, mutation of either the three Twist motifs in *m5/m8* or the two Dorsal motifs produced a delay in the start of transcription in both WT and *eve2-NICD* embryos. These effects were even more pronounced when both Twist and Dorsal motifs were mutated together (Fig. 6**AB**), implying that, without Twist or Dorsal, *m5/m8* requires a higher threshold of NICD to become active or responds more slowly to the same threshold. The mean transcription levels were also reduced in all cases (Fig. 6**A**).

Mutating the Twist motifs had two additional effects: the overall proportion of active cells in the MSE was reduced (Fig. 6**C**) and out of those active, fewer exhibited the sustained profile observed with the wild type enhancers (Fig. 6**DE**). Instead most cells displayed a 'bursty' transcription profile (Fig. 6**D**), similar to those elicited by NICD in the DE region. Although the mutated Twist motifs led to bursty profiles in wild type embryos, these effects were partially rescued when ectopic NICD was provided (Fig. 6**CE**, S6**C**). However, when both Dorsal and Twist motifs were mutated, the proportions of active cells and of cells with a sustained profile were both decreased even in the presence of ectopic NICD (although mutation of Dorsal motifs alone did not produce a significant decrease in either property) (Fig. 6**CE**, S6**C**). The results are therefore consistent with a role for Twist and Dorsal in priming the *m5/m8* enhancer to produce sustained activity. In their absence the ability of the enhancer to initiate transcription becomes much more stochastic. Consistently, another Notch responsive enhancer that only contains one Twist motif (the neuroectodermal enhancer *m8NE*, Fig. S6**A**) also exhibited a delayed onset of activity (Fig. S6**D**) and gave stochastic bursting patters (Fig. 6**E**). This suggest that the two MSE enhancers are especially primed to respond in a fast and sustained manner at this stage.

Discussion

Developmental signaling pathways have widespread roles but currently we know relatively little about how the signaling information is decoded to generate the right transcriptional outcomes. We therefore set out to investigate the principles that govern how Notch activity is read by target enhancers in the living animal, using the MS2/MCP system to visualize nascent transcripts in *Drosophila* embryos and focusing on two enhancers that respond to Notch activity in the MSE. Three striking characteristics emerge. First, the MSE enhancers are sensitive to changes in the levels of NICD, which modulate the transcriptional burst size rather than increasing burst frequency. Second, the activation of both MSE enhancers is highly synchronous. Indeed, within one nucleus the two enhancers become activated within a few minutes of one another. Third, both MSE enhancers confer a sustained response in the wild-type context. This synchronized and persistent activity of the MSE enhancers is in stark contrast to the highly stochastic and bursty profiles that are characteristics of most other enhancers that have been analyzed (Little et al. 2013; Fukaya et al. 2016; Fritzsch et al. 2018) and relies on the MSE enhancers being "primed" by regional transcription factors Twist and Dorsal. We propose that such priming mechanisms are likely to be of general importance for rendering enhancers sensitive to signals so that a rapid and robust transcriptional response is generated.

Priming of enhancers sensitizes the response to NICD

Transcription of most genes in animal cells occurs in bursts interspersed with refractory periods of varying lengths, that are thought to reflect the kinetic interactions of the enhancer and promoter (Bartman et al. 2016). However, the MSE enhancers maintain transcription for 40-60 minutes, without any periods of inactivity. Calculation of the autocorrelation function in the traces from these nuclei suggest very slow transcriptional dynamics (Fig. S4**ED**)(Desponds et al. 2016), which would be consistent with one long period of activity as opposed to overlapping short bursts. This fits with a model where promoters can exist in a permissive active state, during which many "convoys" of polymerase can be fired without the promoter reverting to a fully inactive condition (Tantale et al. 2016). The rapid successions of initiation events are thought to require Mediator complex (Tantale et al. 2016), which was also found to play a role in the NICD-mediated increase in residence time of CSL complexes (Gomez-Lamarca et al. 2018). We propose therefore that the sustained transcription from *m5/m8* and *sim* reflects a switch into a promoter permissive state, in which general transcription factors like Mediator remain associated with the promoter so long as sufficient NICD is present, allowing repeated re-initiation.

However, the ability to drive fast and sustained activation is not a property of NICD itself. For example,

when ectopic NICD was supplied, cells in many regions of the embryo responded asynchronously and underwent only short bursts of activity. Furthermore, variable and less sustained cell-by-cell profiles were generated in the MSE region when the binding motifs for Twist and Dorsal in the *m5/m8* enhancer were mutated. The presence of these regional factors therefore appears to sensitize the enhancers to NICD, a process we refer to as enhancer priming. This has two consequences. First, it enables all nuclei to respond rapidly to initiate transcription in a highly coordinated manner once NICD reaches the threshold level. Second, it creates an effective 'state transition' so that the presence of NICD can switch the promoter into a permissive condition to produce sustained activity (Fig. 7). We propose a priming mechanism, rather than classic cooperativity, because Twist and Dorsal alone are insufficient to drive any enhancer activity. Furthermore, since the enhancers immediately achieve sustained activity when NICD is produced, it is most likely that Twist and Dorsal are required prior to the recruitment of NICD, although both may continue to play a role independently of priming after transcription is initiated, as suggested by the lower mean levels obtained when only Twist or Dorsal motifs are mutated.

Our explanation that the synchronous activation of the MSE enhancers reflects their requirements for a critical concentration of NICD is borne out by their responses when the levels of NICD are increased. Notably, while *sim* and *m5/m8* exhibited almost identical dynamics in wild-type embryos, they displayed clear differences in the presence of ectopic NICD, suggesting that they detect slightly different thresholds. Indeed, doubling the dose of ectopic NICD further accelerated the onset times of *sim* in agreement with the model that the enhancers detect NICD levels. Threshold detection does not appear to rely on the arrangement of CSL motifs, as the onset times of *m5/m8* or *sim* were unaffected by changes in the spacing of CSL paired sites. In contrast, mutating Twist or Dorsal binding-motifs in *m5/m8* delayed the onset of transcription, arguing that these factors normally sensitize the enhancer to NICD enabling responses at lower thresholds.

We propose that enhancer priming will be widely deployed in contexts where a rapid and consistent transcriptional response to signaling is important, as in the MSE where a stripe of cells with a specific identity is established in a short time-window. In other processes where responses to Notch are more stochastic, as during lateral inhibition, individual enhancers could be preset to confer different transcription dynamics. This appears to be the case for a second enhancer from *E(spl)-C* (*m8NE*) which generates a stochastic response in the MSE cells, similar to that seen for the MSE enhancers when Twist and Dorsal sites are mutated. This illustrates that the presence or absence of other factors can toggle an enhancer between conferring a stochastic or deterministic response to signalling.

NICD regulates transcription burst size

Manipulating the levels of NICD revealed that the Notch responsive enhancers act as analog devices that can measure and broadcast variations in levels. Increased NICD levels have a consistent effect on enhancer activity irrespective of the priming state of the enhancer, in all cases leading to an increase in the burst duration. The effects can be most readily quantified in regions where NICD elicits discrete bursts of transcription initiation, such as the dorsal ectoderm for *m5/m8* or mesoderm for *sim* and *m8NE*. Transcriptional bursting has been formalized as a two-state model where the promoter toggles between on and off states, conferring a transcription initiation rate when on(Peccoud et al. 1995; Larson et al. 2009). Changes in the duration or frequency of the bursts lead to an overall increase in transcription. Most commonly, differences in the activity of enhancers have been attributed to changes in the probability of the enhancer switching on (K_{on}), which produces different off periods between bursts, leading to changes in burst frequency (Larson et al. 2013; Senecal et al. 2014; Fukaya et al. 2016; Fritzsch et al. 2018; Lammers et al. 2018; Berrocal et al. 2018). We were therefore surprised to find that higher doses of NICD did not increase the burst frequency. Instead they produced bigger bursts, both by increasing the bursting amplitude, equivalent to the rate of transcription initiation, and the bursting length, indicative of the total time the enhancer stays in the on state. Modifications to the CSL motifs also impact on the same parameters. Thus, enhancers with paired motifs (SPS), which favour NICD dimerization (Nam et al. 2007), produced larger transcription bursts than those where the motifs are further apart. This suggests that paired motifs can 'use' the NICD present more efficiently. Interestingly, even though *m5/m8* and *sim* contain different arrangements and numbers of CSL motifs they have converged to produce the same mean levels of transcription in wild type embryos.

Two models would be compatible with the observations that effective NICD levels alter the burst size. In the first model, increasing the concentration of NICD when the enhancer is activated would create larger Pol II clusters. This is based on the observation that low complexity activation domains in transcription factors can form local regions of high concentration of transcription factors, so-called "hubs", which in turn are able to recruit Pol II (Mir et al. 2017; Tsai et al. 2017; Lu et al. 2018). As the lifetime of Pol II clusters appears to correlate with transcriptional output (Cho et al. 2016), the formation of larger Pol II clusters would in turn drive larger bursts. In the second model, NICD would be required to keep the enhancer in the ON state, for example by nucleating recruitment of Mediator and/or stabilizing a loop between enhancer and promoter, which would in turn recruit Pol II in a more stochastic manner. General factors such as Mediator have been shown to coalesce into phase-separated condensates that compartmentalize the transcription apparatus (Cho et al. 2018; Sabari et al. 2018; Boija et al. 2018) and these could form in a NICD dependent manner. Whichever the mechanism, the clusters/ON state must

persist in a state that requires NICD yet is compatible with NICD having a short-lived interaction with its target enhancers (Gomez-Lamarca et al. 2018). Furthermore, the fact that the activity of *m5/m8* enhancer saturates with one *eve2-NICD* construct, and can't be enhanced by providing a more active promoter, suggests that that there is a limit to the size or valency of the clusters that can form.

Although unexpected, the ability to increase burst size appears to be a conserved property of NICD. Live imaging of transcription in response to the Notch homologue, GLP-1, in the *C.elegans* gonad also shows a change in burst size depending on the signalling levels (Lee et al. 2018). As the capability to modulate burst size is likely to rely on the additional factors recruited, the similarities between the effects in fly and worm argue that a common set of core players will be deployed by NICD to bring about the concentration-dependent bursting properties.

Materials and Methods

Cloning and transgenesis

Generation of MS2 reporter constructs

MS2 loops were placed upstream of a *lacZ* transcript and both were driven using different combinations of enhancers and promoters. 24 *MS2* loops were cloned from *pCR4-24XMS2SL-stable* (Addgene #31865) into *pLacZ2-attB* (Bischof et al. 2013) using *Eco*RI sites. The *m5/m8*, *sim* and *m8NE* enhancers (Zinzen et al. 2006a; Kramatschek et al. 1994) were amplified from genomic DNA and cloned into *pattB-MS2-LacZ* using *Hin*dIII/*Age*I sites (primers in Table 1). Subsequently the promoters *hsp70*, *peve*, *pm5*, *pm6*, *pm7*, *pm8* and *psimE* were cloned by Gibson Assembly (Gibson 2011) in *pattB-m5/m8-MS2-LacZ*, *pattB-sim-MS2-LacZ* and/or *pattB-m8NE-MS2-LacZ* (primers in Table 1) using the *Age*I restriction site and incorporating a *Eag*I site. All mutations introduced in *m5/m8* or *sim* were first introduced by Gibson Assembly in the enhancers contained in *pCR4* plasmids and then transferred to *pattB-peve-MS2-lacZ* using *Hin*dIII and *Age*I sites.

Su(H), Twi, dl and Sna binding motifs were identified using ClusterDraw2 using the PWM from the Jaspar database for each transcription factor. Motifs with scores higher than 6 and pvalues 0.001 were selected. Primers to create sim^{SPS}, $m5/m8^{insSPS}$, $m5/m8^{\Delta twi}$, $m5/m8^{\Delta dl}$ and $m5/m8^{\Delta twi\ \Delta dl}$ are detailed in Table 1.

The following constructs have been generated and inserted by ΦC31 mediated integration (Bischof et al. 2007) into an *attP* landing site in the second chromosome – *attP40*, 25C – to avoid positional effects in the comparisons: *pattB-m5/m8-peve-MS2-LacZ*, *pattB-m5/m8-hsp70-MS2-LacZ*, *pattB-m5/m8-pm5-MS2-LacZ*, *pattB-m5/m8-pm6-*

MS2-LacZ, *pattB-m5/m8-pm7-MS2-LacZ*, *pattB-m5/m8-pm8-MS2-LacZ*, *pattB-m5/m8-psimE-MS2-LacZ*, *pattB-sim-peve-MS2-LacZ*, *pattB-sim-psimE-MS2-LacZ*, *pattB-sim^{SPS}-peve-MS2-LacZ*, *pattB-m5/m8^{insSPS}-peve-MS2-LacZ*, *pattB-m5/m8$^{\Delta twi}$-peve-MS2-LacZ*, *pattB-m5/m8$^{\Delta dl}$-peve-MS2-LacZ* and *pattB-m5/m8$^{\Delta twi\ \Delta dl}$-peve-MS2-LacZ*.

Expression of ectopic NICD

To generate *eve2-NICD* the plasmid 22FPE (Kosman et al. 1997), which contains 2 copies of the *eve2* enhancer with five high affinity *bicoid* sites, FRT sites flanking a transcription termination sequence and the *eve 3'UTR*, was transferred to *pGEM-t-easy* using *Eco*RI sites and from there to *pattB* (Bischof et al. 2013) using a *Not*I site. The NICD fragment from Notch was excised from an existing *pMT-NICD* plasmid and inserted in *pattB-22FPE* through the *Pme*I site to create the *pattB-eve2x2-peve-FRT-STOP-FRT-NICD-eve3'UTR* construct (referred to as *eve2-NICD*). This was inserted into the *attP* landing site at 51D in the second chromosome. To increase the amount of ectopic NICD produced, the same *eve2-NICD* construct was also inserted in the *attP40* landing site at 25C and recombined with *eve2-NICD*51D to produce 2x*eve2-NICD*. Sequences of all generated plasmids are available in a benchling repository.

Fly strains and genetics

To observe the expression pattern and dynamics from *m5/m8-peve*, *sim-peve* and the different promoter combinations (Fig. 1, S1) females expressing His2av-RFP and MCP-GFP (BDSC #60340) in the maternal germline were crossed with males expressing the *MS2-lacZ* reporter constructs.

To test expression from *m5/m8-peve* in the *Dl* and *neur* mutant backgrounds, *His2Av-RFP* from *His2av-RFP ; nos-MCP-GFP* (BDSC #60340) was recombined with *nos-MCP-GFP* in the second chromosome (BDSC #63821) and combined with a deficiency encompasing the *Dl* gene (*Df(3R)Dl^{FX3}*, (Vässin et al. 1987)) or a *neuralized* loss of function allele (*neur$^{[11]}$*, BDSC #2747). *m5/m8-peve-MS2-lacZ* was also combined with the *Dl* and *neur* alleles and mutant embryos were obtained from the cross *His2Av-RFP,nos-MCP-GFP ; mut / TTG* x *m5/m8-peve-MS2-lacZ ; mut / TTG*. Homozygous mutant embryos for *Dl* or *neur* were selected by the lack of expression from the *TTG* balancer (*TM3-twi-GFP*).

To observe transcripion from two MS2 reporters in each cell (Fig. 2, S2) *His2Av-RFP* (BDSC #23650) was recombined with *nos-MCP-GFP* (from BDSC #60340) in the third chromosome and combined with *m5/m8-peve* or *sim-peve* MS2 reporters. *m5/m8-peve* x2 embryos and *sim-peve* x2 embryos were obtained from the

stocks *m5/m8-peve-MS2-LacZ ; His2Av-RFP,nos-MCP-GFP* and *sim-peve-MS2-LacZ ; His2Av-RFP,nos-MCP-GFP*, respectively; while *m5/m8-peve + sim-peve* embryos were obtained from crosssing *sim-peve-MS2-LacZ ; His2Av-RFP,nos-MCP-GFP* females with *m5/m8-peve-MS2-LacZ* males.

To observe transcription from MS2 reporters in conditions of ectopic Notch activity the *FRT-STOP-FRT* cassette had to be first removed from the *eve2-NICD* construct by expression of a flippase in the germline. To do so flies containing *ovo-FLP* (BDSC #8727), *His2Av-RFP* and *nos-MCP-GFP* were crossed with others containing *eve2-FRT-STOP-FRT-NICD*, *His2Av-RFP* and *nos-MCP-GFP*. The offspring of this cross (*ovo-FLP/+ ; eve2-FRT-STOP-FRT-NICD/+ ; His2Av-RFP, nos-MCP-GFP*) induced FRT removal in the germline and were crossed with the MS2 reporters to obtain embryos expressing ectopic NICD. We note that only half of the embryos present the *eve2-NICD* chromosome, which could be distinguished by ectopic MS2 activity and an ectopic cell division of all the cells in the eve2 stripe after gastrulation. The other 50% embryos obtained from this cross were used as the wild type controls. This strategy was used to observe transcription from *m5/m8-peve*, *sim-peve*, *m8NE-peve*, *m5/m8-pm5*, sim^{SPS}*-peve*, *m5/m8*^{insSPS}*-peve*, *m5/m8*$^{\Delta twi}$*-peve*, *m5/m8*$^{\Delta dl}$*-peve* and *m5/m8*$^{\Delta twi\ \Delta dl}$*-peve*. To measure transcription from 2x*eve2-NICD* (Fig. 4, S4) removal of the *FRT-STOP-FRT* cassete was induced from the male germline to avoid recombination. To do so, *betaTub85D-FLP* (BDSC #7196) females were crossed with 2x*eve2-NICD* males and the male offspring of this cross (*betaTub85D-FLP/Y ; 2xeve2-NICD/+*), which induces FRT removal in the germline, were crossed with *m5/m8-peve-MS2-lacZ ; His2AvRFP, nos-MCP-GFP* or *sim-peve-MS2-lacZ ; His2AvRFP, nos-MCP-GFP* females. As in the previous strategy, only half of the embryos presented the 2x*eve2-NICD* chromosome and were distinguished by the ectopic activity.

Live imaging

Embryos were dechorionated in bleach and mounted in Voltalef medium (Samaro) between a semi-permeable membrane and a coverslip. The ventral side of the embryo was facing the coverslip in all movies except when looking at transcription in the DE region (Fig. 3**B**, S4**AC**), in which they were mounted laterally. Movies were acquired in a Leica SP8 confocal using a 40x apochromatic 1.3 objective and the same settings for MCP-GFP detection: 40mW 488nm argon laser detected with a PMT detector, pinhole airy=4. Other settings were slightly different depending on the experiment. To observe transcription in the whole embryo (Fig. 1) settings were: 3% 561nm laser, 0.75x zoom, 800x400 pixels resolution (0.48um/pixel), 19 1um stacks, final temporal resolution of 10 seconds/frame). To observe transcription from 2 MS2 alleles simultaneously (Fig. 2) settings were: 2% 561nm laser, 1.5x zoom, 800x400 pixels resolution (0.24um/pixel), 29 1um stacks, final temporal resolution of 15s/frame). In all experiments with ectopic NICD a ~150x150um window anterior to the center of the embryo was captured.

Settings were: 2% 561nm laser, 2x zoom, 400x400 pixels resolution (0.36um/pixel), 29 1um stacks, final temporal resolution of 15s/frame). All images were collected at 400Hz scanning speed in 12 bits.

Image analysis

Movies were analyzed using custom Matlab (Matlab R2018a, Mathworks) scripts (available at GitHub:FryEmbryo3DTracking Briefly, the His2Av-RFP signal was used to segment and track the nuclei in 3D. Each 3D stack was first filtered using a median filter, increasing the contrast based on the profile of each frame to account for bleaching and a fourier transform log filter (Garcia et al. 2013). Segmentation was performed by applying a fixed intensity threshold, 3D watershed accounting for anisotropic voxel sizes (Mishchenko 2015) to split merged nuclei and thickening each segmented object. Nuclei were then tracked by finding the nearest object in the previous 2 frames which was closer than 6 um. If no object was found, that nuclei was kept with a new label, and only one new object was allowed to be tracked to an existing one. After tracking, the 3D shape of each nucleus in each frame was used to measure the maximum fluorescence value in the GFP channel, which was used as a proxy of the spot fluorescence. We note than when a spot cannot be detected by eye this method detects only background, but the signal:background ratio is high enough that the subsequent analysis allows to classify confidently when the maximum value is really representing a spot.

In experiments with two MS2 reporters the maximum intensity pixel per nucleus does not allow to separate transcription from the two alleles. To do so, the 3D Gaussian spot detection method from(Garcia et al. 2013) was implemented in the existing tracking, such that each spot was segmented independently and associated with the overlapping nuclei. In this manner only active transcription periods were detected and no further processing of the traces was required.

MS2 data processing

From the previous step we obtained the fluorescent trace of each nuclei over time. Only nuclei tracked for more than 10 frames were kept. First nuclei were classified as inactive or active. To do so the average of all nuclei (active and inactive) was calculated over time and fitted to a straight line. A median filter of 3 was applied to each nuclei over time to smooth the trace and ON periods were considered when fluorescent values were 1.2 times the baseline at each time point. This produced an initial classification of active (nuclei ON for at least 5 frames) and inactive. Using these inactive nuclei, the mean fluorescence from MCP-GFP was fitted again to redefine the baseline and active:inactive nuclei were classified again. Nuclei were then classified as MSE or earlier stages and the MSE ones were kept for further analysis.

The final fluoresncent values for each nuclei were calculated by removing the fitted baseline from the maximum intensity value for each and normalizing for the percentage that the MCP-GFP fluorescence in inactive nuclei decreases over time to account for the loss of fluorescence due to bleaching.

In all movies time into nc14 was considered from the end of the 13th syncythial division. When this was not captured they were synchronized by the gastrulation time.

Each nucleus was classified into the 4 regions (ME, MSE, NE and DE) by drawing rectangular shapes in a single frame and finding which centroids overlapped with each region. In *eve2-NICD* these regions along the DV axis were defined within the *eve2* stripe ($\sim$ 6-7 cells wide in all movies). In wild type embryos ME and MSE regions were drawn in the whole field of view ($\sim$ 150x150 um anterior half of the embryo).

Definition of bursting properties

Bursts were defined as periods were the median filtered signal was higher than 1.2 times the baseline for at least 5 frames after the initial burst of activity at the beginning of nc14 (the considered period started at 15 min into nc14). These defined the burst duration and the time off between bursts. The amplitude was defined as the mean value within each burst period.

Onsets and ends of transcription were defined as the beginning of the first burst and the end of the last respectively (also starting at 15 min into nc14). In Fig. 2 to be more precise in measuring the onsets and end-points of transcription for both MS2 alleles they were scored manually as the first and last frame a spot is detected and randomly assigned 'allele 1' or 'allele 2'. The total variability was the variance of all onsets or end points, combining both alleles. The extrinsic variability was calculated as the covariance of onsets and ends between alleles 1 and 2. The remaining (total - covariance) corresponds to the intrinsic variability within each cell.

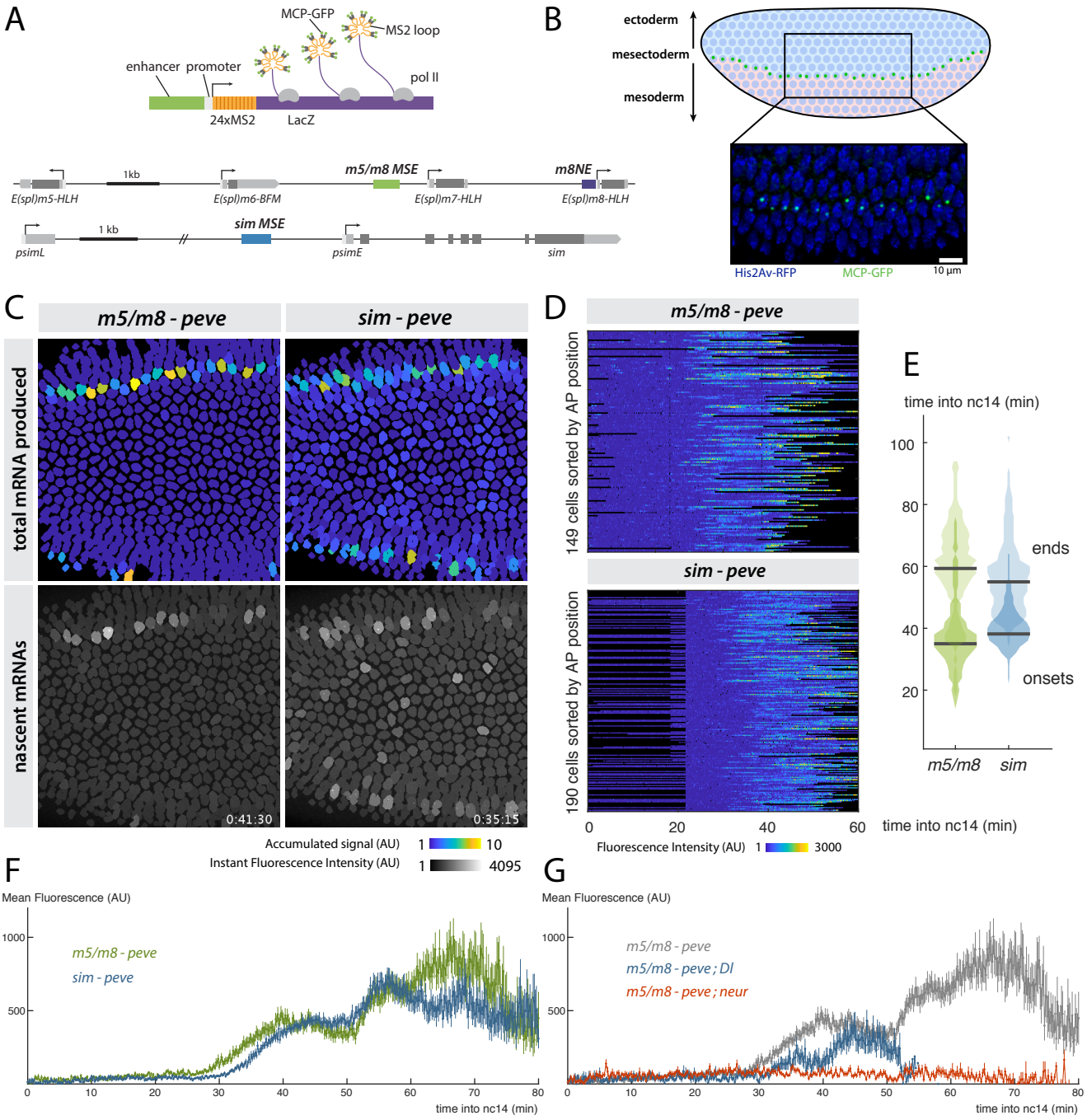

Figure 1. Synchronous activity of two Notch responsive enhancers. A) Diagrams illustrating the strategy for live imaging of transcription using the MS2 system (top) and the location of mesectoderm (MSE) and neuroectoderm (NE) enhancers from the *E(spl)*locus (*m5/m8*, green and *m8NE*, purple) and *single minded* gene (*sim*, blue) (bottom). Arrows indicate promoters/transcription start-sites and boxes in lower panel indicate non-coding (light grey) and coding (dark grey) transcribed regions. **B**) Diagram of a blastoderm *Drosophila* embryo, indicating region of Delta expression (pink) in the mesoderm which activates the Notch pathway in a flanking stripe of cells (green dots) to specify the MSE. Transcription from the *m5/m8* reporter is detected in each of the cells in the stripe by accumulation of MCP-GFP in bright puncta at the transcription site (see panel where nuclei are labelled by His2Av-RFP, blue). **C**) Tracked expression from *m5/m8* and *sim* reporters. Top panels: tracked nuclei are false-colored by their total signal levels, proportional to their total mRNA production, showing that both *m5/m8* and *sim* direct expression in 1-cell wide MSE stripes. Bottom panels: single frame of *m5/m8* and *sim* embryos. Tracked nuclei are shaded by their maximum pixel intensity in that frame (timestamp indicates minutes into nc14). In addition to MSE cells, *sim* also exhibits low sporadic activity in some mesodermal cells. **D**) *m5/m8* and *sim* initiate transcription synchronously in all MSE cells. Heat-maps representing time-course during nc14 of all fluorescence traces from MSE cells in *m5/m8* and *sim* embryos (scale as indicated where blue is no expression and yellow

Figure 1 (continued). is high expression; black indicates periods where nuclei were not tracked). Transcription begins within 30-35 min into nc14. **E**) Distributions of onsets and end-points of transcription from *m5/m8* (green) and *sim* (blue) in MSE cells. Transcription starts synchronously in a 10 minute window from 30 min into nc14 and is extinguished 30 to 60 min afterwards. **F**) *m5/m8* (green) and *sim* (blue) produce similar average temporal profiles. Mean fluorescent intensity of MCP-GFP puncta, (arbitrary units, AU) at the indicated times after start of nc14. **G**) Transcription from *m5/m8* is curtailed in embryos lacking zygotic production of Delta (Dl, blue) and abolished in embryos lacking neuralized (neur; red). Grey trace is profile from *m5/m8* in wild-type embryos shown in **F**. In **F** and **G** mean and SEM of all MSE cells are shown. n = 3 (*m5/m8*), 3 (*sim*), 2 (*m5/m8 ; Dl*), 2 (*m5/m8 ; neur*) embryos.

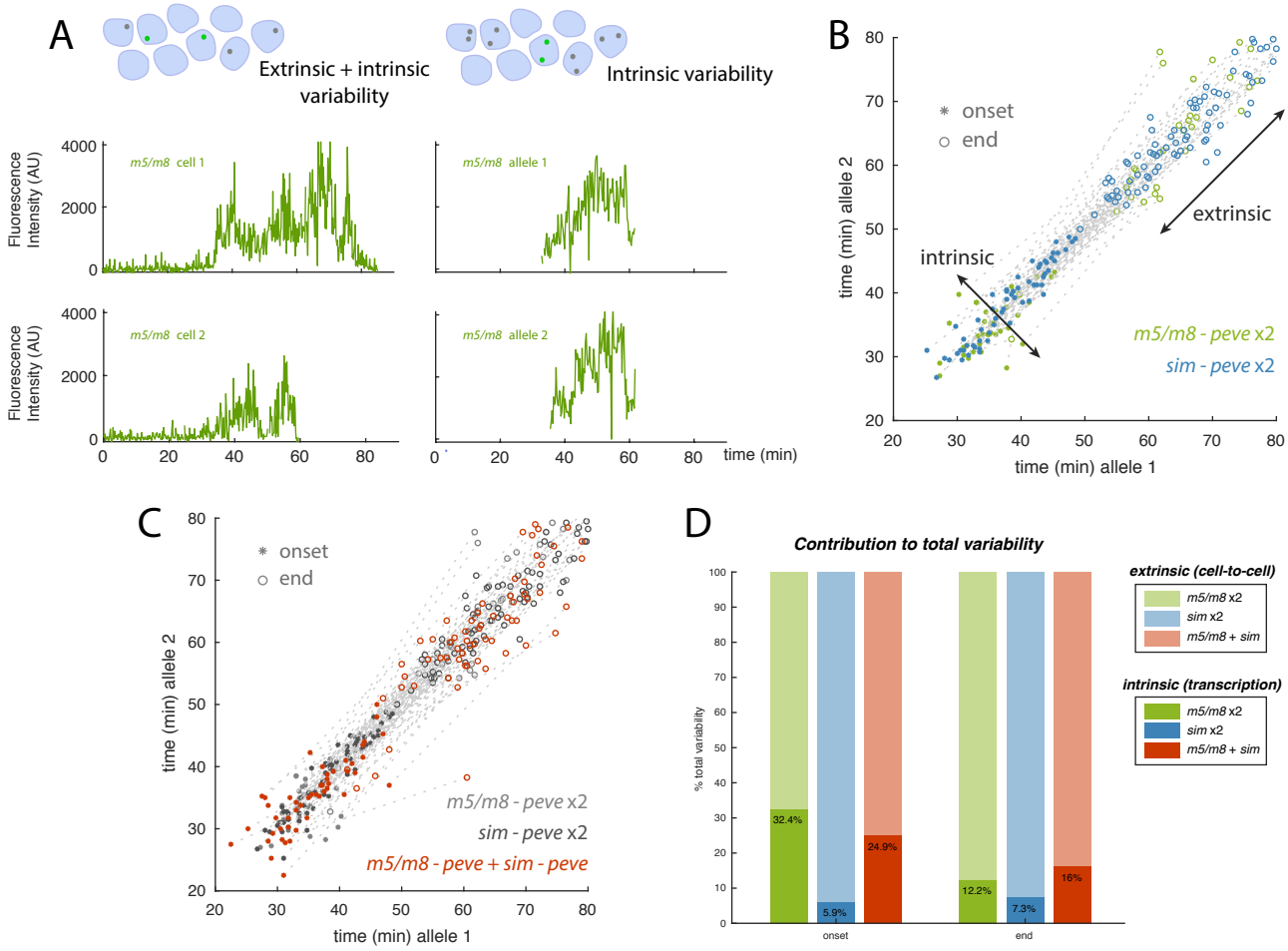

Figure 2. Notch enhancers exhibit low intrinsic variability. **A**) Examples of fluorescence traces from different cells (left panels) where variability is due to the effects of extrinsic (e.g. signaling, cell-to-cell variability in other factors) and intrinsic (due to the stochastic nature of transcription) variability. Examples of fluorescence traces from two alleles in the same cell (right panels) illustrating low intrinsic transcriptional variability between the enhancers. **B**) *m5/m8* and *sim* both exhibit low intrinsic variability in their onset and end-point of activity. Fluorescence intensity from individual puncta was quantified in nuclei carrying two alleles of *m5/m8* (green) or *sim* (blue) and their relative onset and end-point of activity plotted. Distribution across the diagonal reflects intrinsic variability (within cells) whereas distribution along the diagonal reflects extrinsic variability (between cells). **C**) *m5/m8* and *sim* exhibit highly correlated activity. Fluorescence intensity from individual puncta was quantified in nuclei carrying an allele of *m5/m8* and an allele of *sim* and their relative onset and end-points plotted (red) (with data from the individual enhancers, **C**, shown in grey for comparison). **D**) Variability intrinsic to transcription (dark shading) contributes a small percentage of the observed total variability in onsets and end-points of transcription from the MSE enhancers, in comparisons of two alleles, as indicated. In **B** and **C** onsets and ends are randomly assigned allele 1 or 2. Connecting grey lines indicates onset and end times come from the same cell. n = 2 (*m5/m8*x2), 3 (*sim*x2), 3 (*m5/m8 + sim*) embryos.

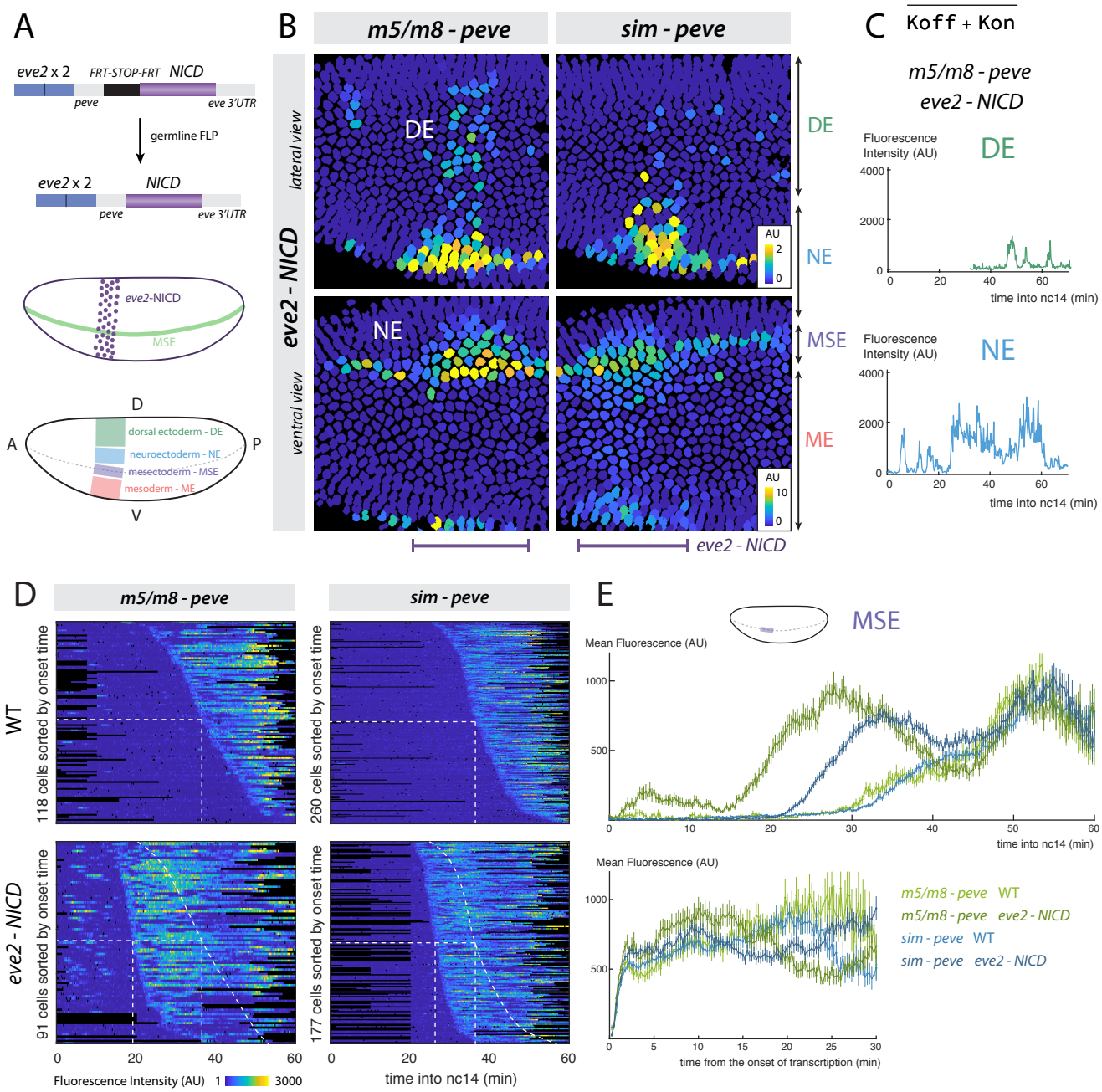

Figure 3. Effects of ectopic NICD on temporal transcription profiles reveals enhancers have different thresholds. A) Diagram illustrating the strategy for producing ectopic NICD in a stripe orthogonal to the MSE using the *eve stripe 2* enhancer (*eve2*), with schematic showing site of expression (purple shading) relative to the MSE stripe (green) and an overview of the regions along the DV axis where the effects on transcription were quantified. **B**) Still frames of tracked nuclei false-colored with the total accumulated signal (note different scales). DE, NE, MSE, ME correspond to the regions shown in **A**. Both *m5/m8* and *sim* have strongest responses in NE/MSE region. *m5/m8* activity is also detected in sporadic dorsal ectoderm (DE) nuclei. Conversely *sim* exhibits low sporadic activity in mesodermal cells (ME). **C**) NICD produces different transcription profiles from *m5/m8* depending on DV cell context, illustrative traces from DE (top) and NE (bottom). **D**) Heatmaps of transcription traces from all MSE cells in *m5/m8* and *sim* in wild type and *eve2-NICD* embryos, sorted by onset time. Both enhancers are active earlier and more synchronously in *eve2-NICD*, with *m5/m8* shifted to a greater extent than *sim*. Dashed lines indicate onset times in wild type embryos. **E**) Mean profiles of activity in MSE nuclei over time (top) and aligning traces by the onset time (bottom). *m5/m8* and *sim* give earlier onsets and higher levels of transcription in *eve2-NICD*. When aligned by onset time transcription increases steeply in all conditions, indicating the gradual mean increase over time reflects the small differences in onset times between nuclei. **E** shows mean and SEM of all MSE cells. n = 4 (*m5/m8* WT), 7 (*sim* WT), 6 (*m5/m8 eve2-NICD*), 8 (*sim eve2-NICD*) embryos.

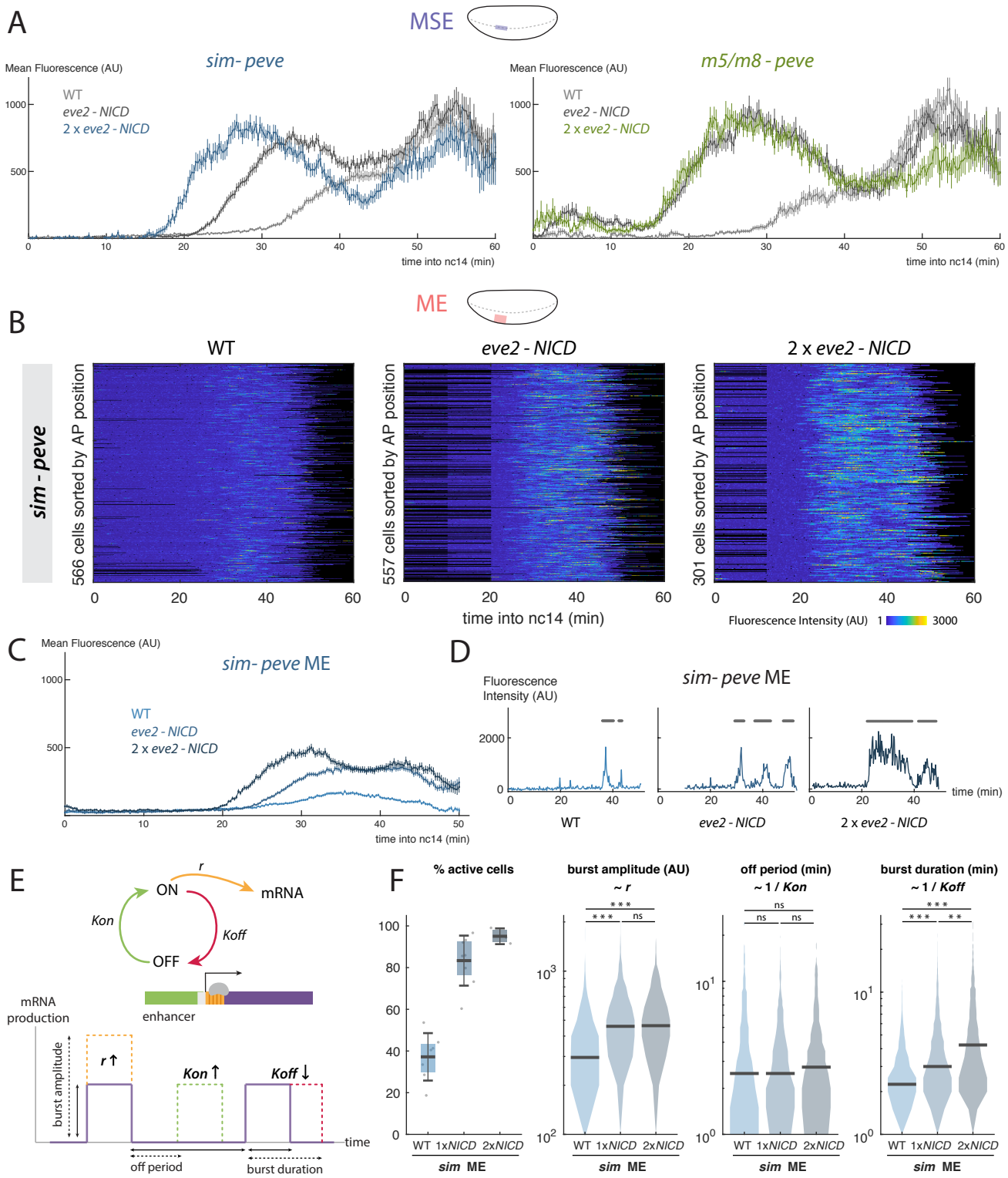

Figure 4. Notch produces a dose-sensitive response by regulating transcription burst size. A) An additional NICD insertion, 2x*eve2-NICD*, elicits earlier and higher transcription from *sim* (blue, left) in MSE cells but does not alter the mean profile from *m5/m8* (green, right) in comparison to 1x*eve2-NICD* (dark grey). Mean levels from wild type (light grey) and 1x*eve2-NICD* (dark grey) embryos are reproduced from Fig. 3**E**. **B**) Heatmaps depicting *sim* activity in ME nuclei in the three conditions as indicated. Note the different scale range compared to Fig. 3**D**. **C**) Ectopic NICD produces a dose-sensitive increase in mean levels of transcription from *sim* in the mesoderm. **D**) Examples of transcription traces from single ME cells in WT, 1x*eve2-NICD* and 2x*eve2-NICD* embryos. Burst periods are marked with a grey line. **E**) Schematic of the model used to describe transcription. An enhancer cycles between ON and OFF states and produces mRNA when

Figure 4 (continued). ON. Changes in the properties of bursting amplidude, off period and bursting duration can be correlated with changes in the kinetic constants r, Kon and $Koff$. **F**) Quantification of the bursting properties of transcription from *sim* in mesodermal cells in wild type, 1x*eve2-NICD* and 2x*eve2-NICD* embryos. The proportion of active cells, the burst amplitude and duration are all increased but the off period is unchanged. Boxplots indicate median, with 25-75 quartiles; error bars are SD. Violin plots, distributions of the analyzed bursts, bar indicates the median. In **A** and **C** mean fluorescence values and SEM are plotted. n cells for **B**-**F** are indicated in **B**. Differential distributions tested with two-sample Kolmogorov-Smirnov test: pvalues <0.01(*), $<10^{-5}$(**), $<10^{-10}$(***). n = 3 (*m5/m8* 2x*eve2-NICD*), 3 (*sim* 2x*eve2-NICD*) embryos.

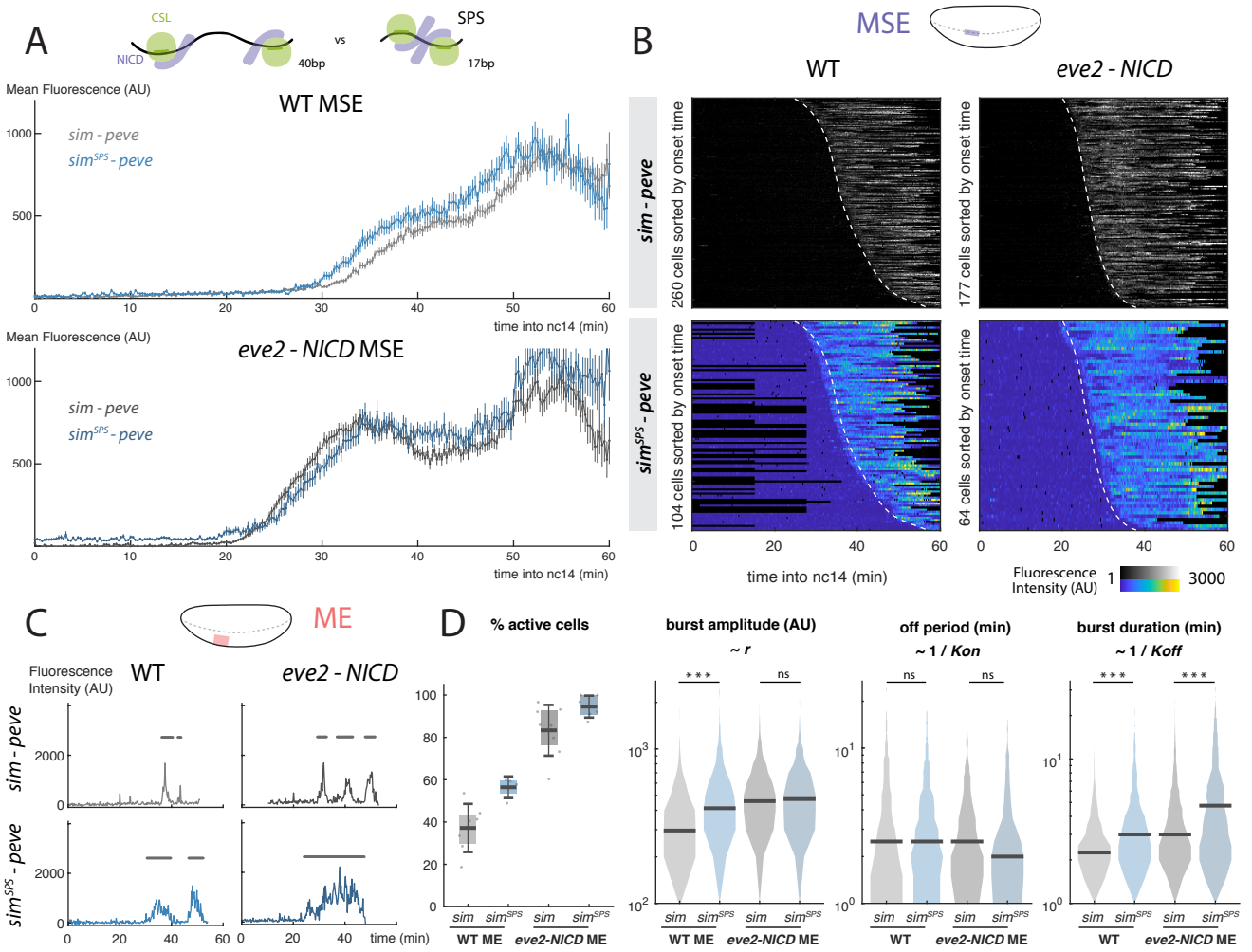

Figure 5. Optimized Su(H) motif organization enhances bursting size. A) Replacing two Su(H) motifs in *sim* with an optimal paired SPS motif sim^{SPS} increases the mean levels of transcription in wild type embryos (top, blue) but does not shift the onset in wild type or *eve2-NICD* embryos (bottom, blue). Mean levels for unmodified *sim* (grey) are from Fig. 3**E**. Mean and SEM for all MSE cells shown. **B**) Heatmaps of transcription in all active MSE cells in the conditions indicated. sim^{SPS} has similar onset to *sim* in wild-type and 1x*eve2-NICD* embryos. Dashed lines indicate onset times in the wild type enhancer. **C**) Examples of fluorescent traces from *sim* (grey) and sim^{SPS} (blue) in ME nuclei. Burst periods are indicated with grey lines. **D**) sim^{SPS} induces transcription in a higher proportion of cells and increases the burst size compared to *sim*. Boxplots indicate median, 25-75 quartiles and errorbars are SD. Violin plots, distribution for all bursts measured in the ME, bar indicates the median. Differential distributions tested with two-sample Kolmogorov-Smirnov test: pvalues <0.01(*), $<10^{-5}$(**), $<10^{-10}$(***). n = 4 (sim^{SPS} WT) and 6 (sim^{SPS} *eve2-NICD*) embryos. Grey lines, heatmaps and violin plots are re-plotted from Fig. 3**DE** and 4**DF** for comparison.

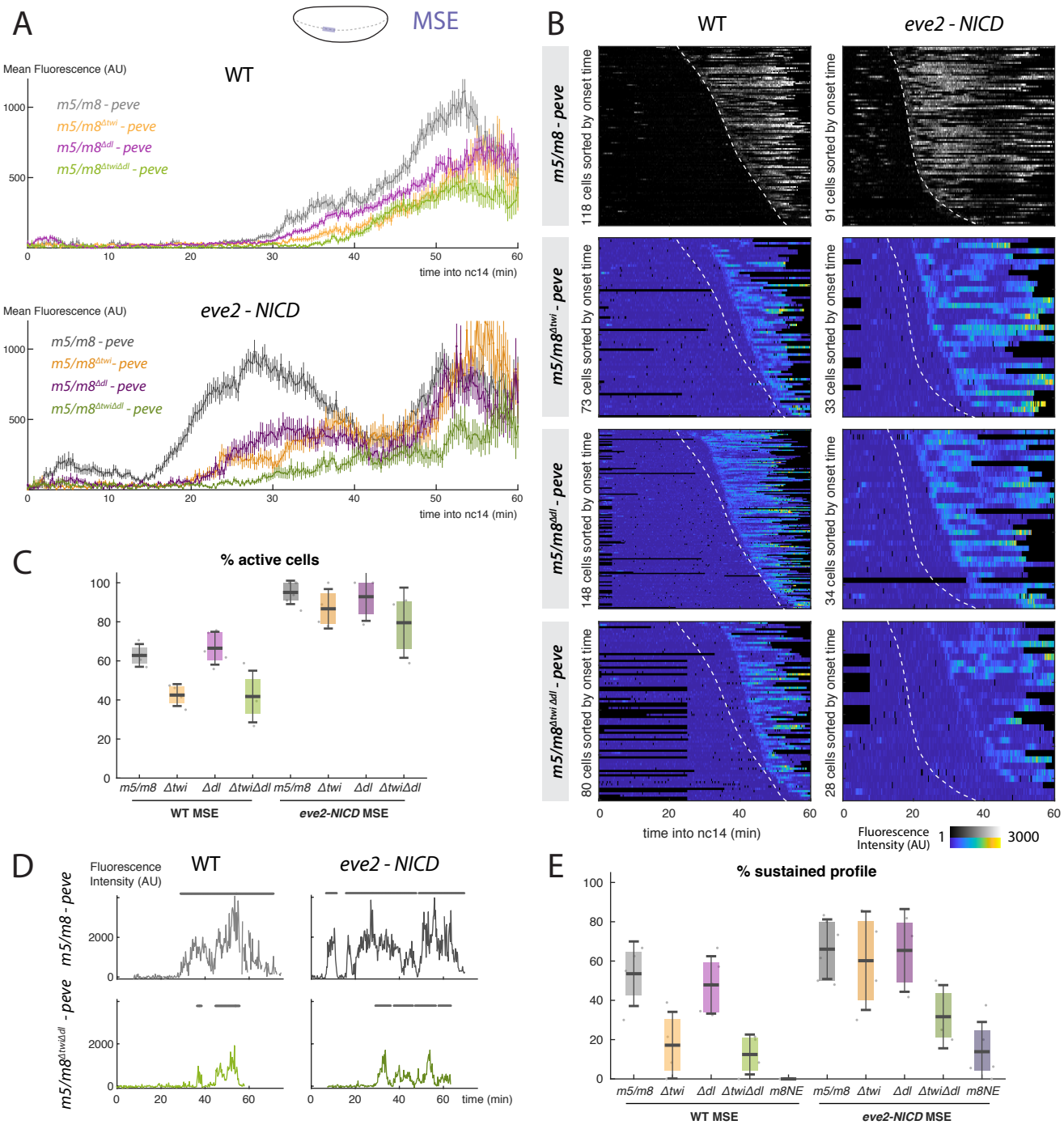

Figure 6. Twist and Dorsal prime the response of *m5/m8* to NICD. A) Mutations in Twist and/or Dorsal binding motifs in *m5/m8* produce delays in the onsets of transcription and lower mean levels of activity in wild type (top) and *eve2-NICD* (bottom) embryos. **B**) Heatmaps of the activity of all MSE cells in the mutated enhancers and in wild type and *eve2-NICD*. The onset of transcription is delayed when Twist and/or Dorsal motifs are mutated. Dashed lines indicate onset times in the wild type enhancer. **C**) Mutations in Twist but not Dorsal motifs reduce the proportion of active cells in wild type embryos. **D**) Examples of transcription traces from MSE cells from the wild type *m5/m8* enhancer and the enhancer with mutated Twist and Dorsal motifs in wild type and *eve2-NICD* embryos. The profiles from $m5/m8^{\Delta twi\Delta dl}$ MSE cells present 'bursty' rather than sustained transcription. ON periods are marked with a grey line. **E**) Quantification of the proportion of MSE cells per embryo displaying a sustained profile of transcription, defined by the presence of at least one burst longer than 10 min. Median, quartiles and SD are shown. Grey lines and heatmaps are re-plotted from Fig. 3**DE**. n = 4 ($m5/m8^{\Delta twi}$ WT), 5 ($m5/m8^{\Delta dl}$ WT), 4 ($m5/m8^{\Delta twi\Delta dl}$ WT), 4 ($m5/m8^{\Delta twi}$ *eve2-NICD*), 3 ($m5/m8^{\Delta dl}$ *eve2-NICD*), 3 ($m5/m8^{\Delta twi\Delta dl}$ *eve2-NICD*), 3 (*m8NE* WT), 5 (*m8NE eve2-NICD*).

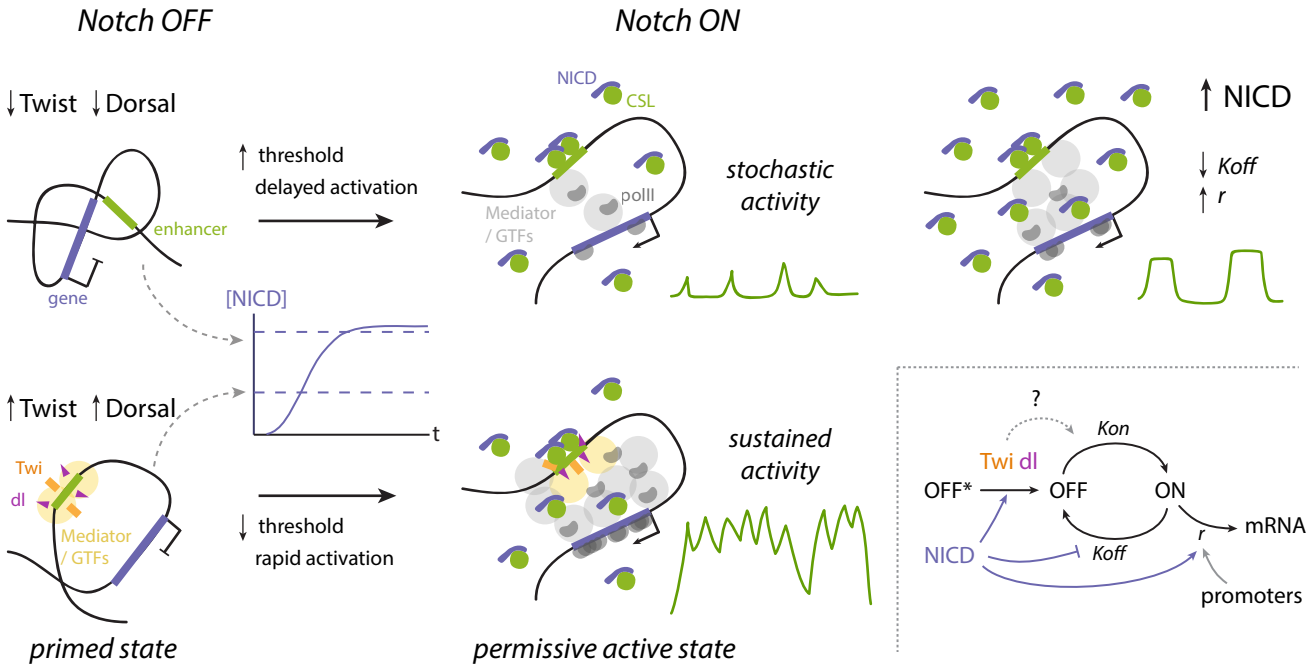

Figure 7. Model of transcriptional regulation by Notch through enhancer priming and burst size modulation. Priming by the tissue-specific factors Twist and Dorsal produces rapid activation in response to NICD and a state transition into a permissive active state in which sustained transcription can be produced without cycling between on and off states. In the absence of these factors stochastic activity is produced in response to NICD. Increasing levels of NICD regulate the overall probability of the enhancer switching on (OFF* to OFF, which is also modulated by Twist and Dorsal), and increase the bursting size (higher r and lower K_{off}). In contrast different promoters control the initiation rate r but do not affect the enhancer activation dynamics. The effects of Twist and Dorsal on enhancer priming might also act by modulating the same parameters of transcription.

Supplemental Information

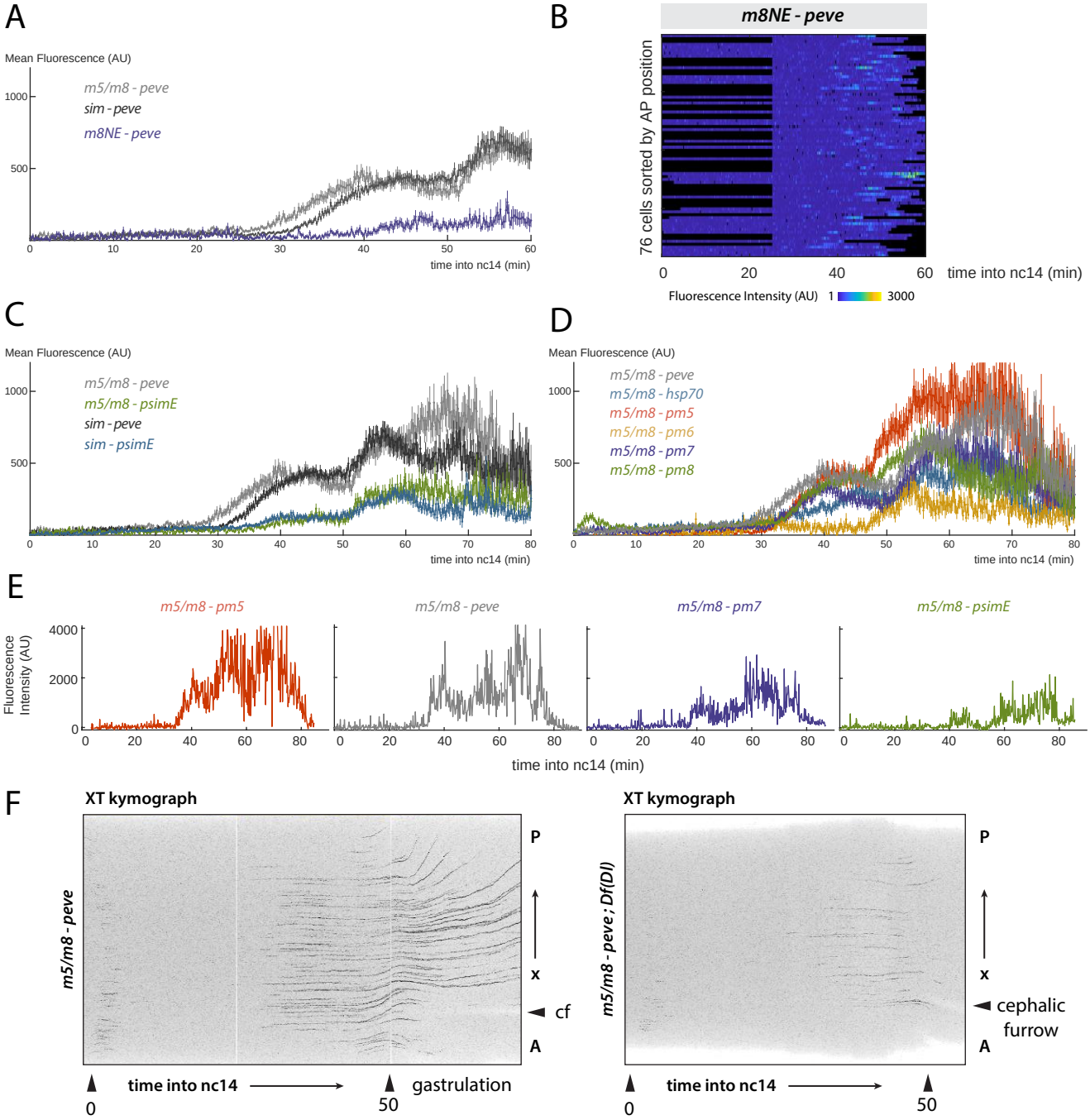

Figure S1. The temporal profile of transcription is characteristic of MSE enhancers. A) A Notch responsive neuroectodermal enhancer (*m8NE*, purple) presents a different temporal pattern than *m5/m8* and *sim*. **B**) *m8NE* produces asynchronized and stochastic transcription in the MSE. **C**) The early promoter of *sim* (*psimE*) produces similar, lower mean levels of transcription from *m5/m8* and *sim* compared to the *eve* promoter. **D**) Different promoters from *E(spl)* complex genes and *hsp70* also affect the mean levels of activity but not the global pattern of transcription. **E**) Examples of fluorescent traces from different promoters. All produce continuous traces of different levels. **F**) Projections of the raw MCP-GFP channel over the Y and Z axes creating an XT kymograph. Only a few cells initiate transcription in embryos lacking zygotic Dl protein (right) compared to wild type embryos (left) and it is extinguished earlier. Mean and SEM are shown in **A**, **C** and **D**. Grey lines are re-plotted from Figs. 1**F** 2**A** for comparison. n = 2 (*m8NE-peve*), 2 (*m5/m8-psimE*), 4 (*sim-psimE*), 3 (*m5/m8-hsp70*), 3 (*m5/m8-pm5*), 3 (*m5/m8-pm6*), 3 (*m5/m8-pm7*), 4 (*m5/m8-pm8*).

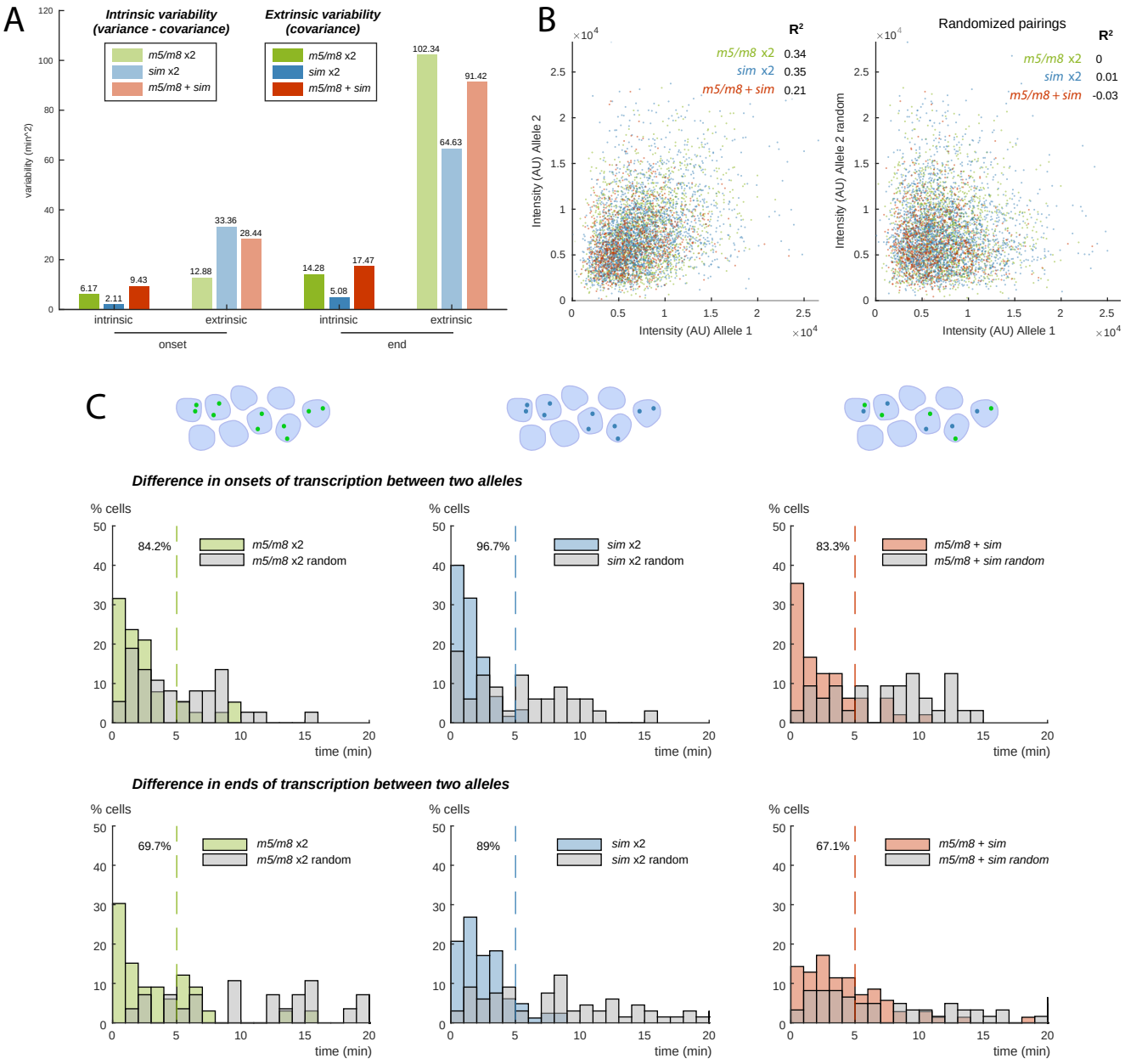

Figure S2. Quantification of the variability intrinsic and extrinsic to transcription. **A**) Intrinsic (total variability minus covariance) and extrinsic (covariance) variability quantified in the onsets and ends of transcription using two MS2 reporters per cell. The amount of intrinsic variability is much smaller than the extrinsic and the intrinsic variability is higher in the ends than onsets of transcription for each combination. **B**) The fluorescence intensities in two alleles at any timepoint present a small but significant correlation (left), compared to a correlation of 0 when the allele pairs are randomly assigned (right). Each color indicates the combination of 2 reporters compared. **C**) Histograms of the time difference between the appearance or dissapearance of transcription foci between the two reporters. The synchrony in the onset times is less than 5 min in more than 80% of the cells and more than 60% in the ends of transcription. Grey bars indicate the distribution of time differences when the allele pairs are randomly assigned.

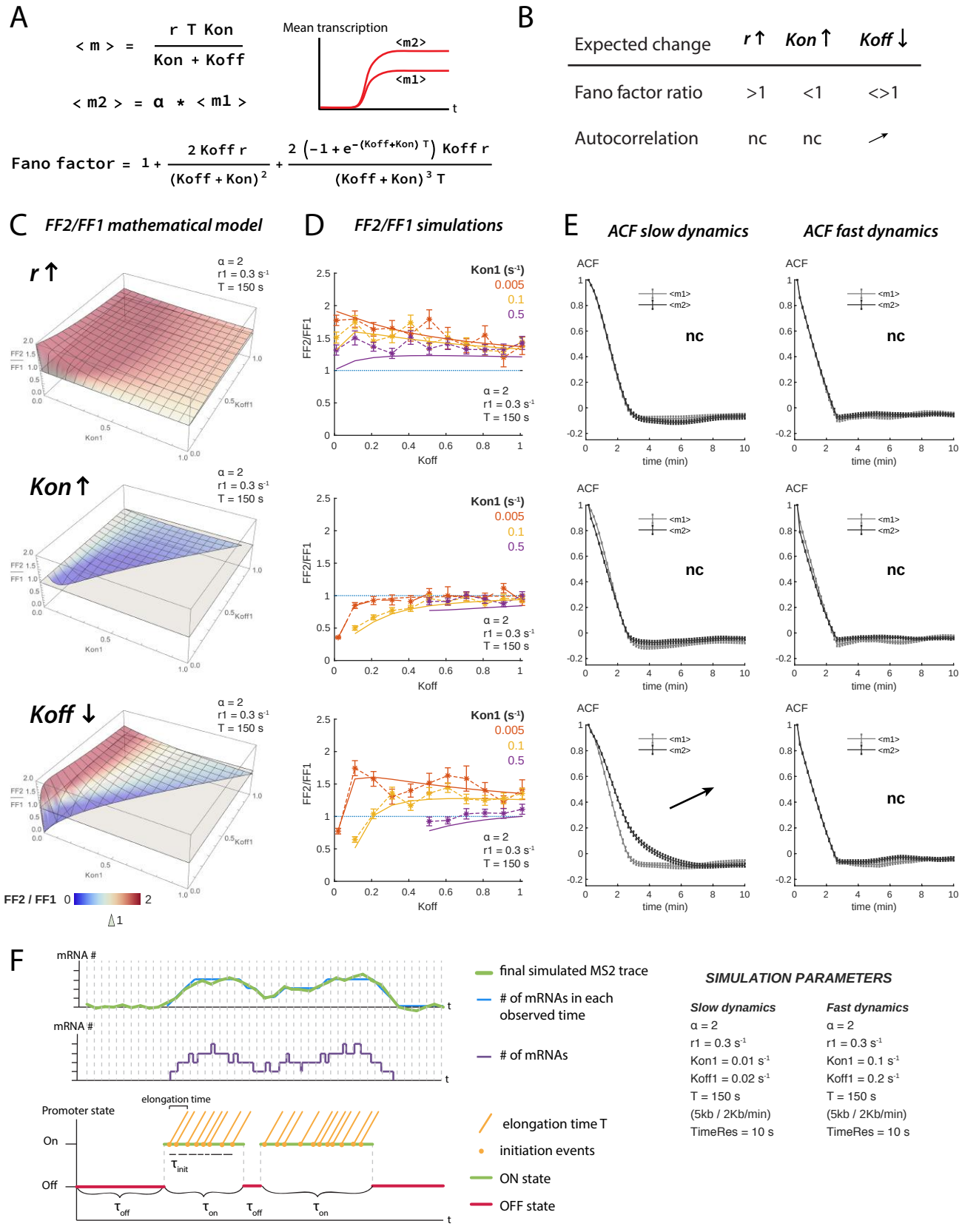

Figure S3. **Modelling a two-state promoter to infer changes in the kinetic parameters of transcription.**

Figure S3 (continued). **A**) Expressions for the mean and Fano factor of the described 2-state model of transcription. Simulations and experiments compare the traces from two populations that have distinct means $\langle m1 \rangle$ and $\langle m2 \rangle$. α is the fold change in mean levels. The mean levels of transcription could increase from an increase in r, increase in K_{on} or decrease in K_{off}. **B**) Summary of the effects that modifying each parameter to produce an increase of α in the mean have on the Fano factor ratio (FFR = FF2/FF1) and autocorrelation function (ACF). When r increases, all FFR values are greater than 1 and no change (nc) in the ACF is observed. When K_{on} increases all FFR values are smaller than 1 and no change is observed in the ACF. When K_{off} decreases FFR values can be greater or smaller than 1 and the ACF presents a shift to the right when the dynamics are slow enough (see below). **C**) 3D plots representing the expected Fano factor ratio values from the mathematical model as a function of K_{on1} and K_{off1}. $\alpha = 2$, $r_1 = 0.3s^{-1}$ and $T = 150s$ in the three plots. The grey surface indicates FFR = 1. Only K_{on1} and K_{off1} values that produce allowed (ie. positive) K_{on2} and K_{off2} values are plotted (see Supplementary Methods for details). Surface map is colored based on FFR values ranging from 0 (blue) to 2 (red). When an increase of α in the mean is caused by an increase in r all FF ratio (FF2/FF1) values for any K_{on} and K_{off} values are greater than 1 (top plot). When it is due to an increase in K_{on} all FF ratios are smaller than 1 (middle plot). When K_{off} decreases to produce an increase of α in the mean, the obtained FF ratio values can be greater or smaller than 1 depending on the starting K_{on1} and K_{off1} parameters (bottom plot). **D**) Comparisons of the Fano factor ratios obtained from simulations of MS2 traces with different parameters (dashed lines) and the predicted from the mathematical model (solid line). Asterisks and error bars are mean and SD of the Fano factor ratio over 50 bootstraps of 1000 simulated MS2 traces, using the described K_{on1} and K_{off1} values and $\alpha = 2$, $r_1 = 0.3s^{-1}$, $T = 150s$ ($5Kb$ / $2Kb/min$). The expected trends in Fano factor ratios are correctly recovered in the simulations of transcription. **E**) Plots showing the changes ACF over time in simulated traces, comparing mean and SD of the ACF of 200 simulated MS2 traces in 50 bootstraps obtained from two groups: $\langle m1 \rangle$, grey, and $\langle m2 \rangle$, black. The parameters used for the simulations are $K_{on1} = 0.01$ and $K_{off1} = 0.02$ (slow dynamics, left column) or $K_{on1} = 0.1$ and $K_{off1} = 0.2$ (fast dynamics, right column) and $\alpha = 2$, $r_1 = 0.3s^{-1}$, $T = 150s$. No changes in the ACF are observed when the dynamics are fast. When the dynamics are slow, increases in r or K_{on} do not produce any change in the ACF but changes decreases in K_{off} shift the ACF to the right, from $\langle m1 \rangle$ to $\langle m2 \rangle$. **F**) Schematic representation of the steps to simulate MS2 traces. First ON and OFF states are generated based on the Gillespie algorithm, ON states are filled with initiation events that spread over their elongation time T. The final trace is obtained by counting the number of initiation events at each of the observed time points and adding gaussian noise to simulate experimental noise (see Supplementary Methods).

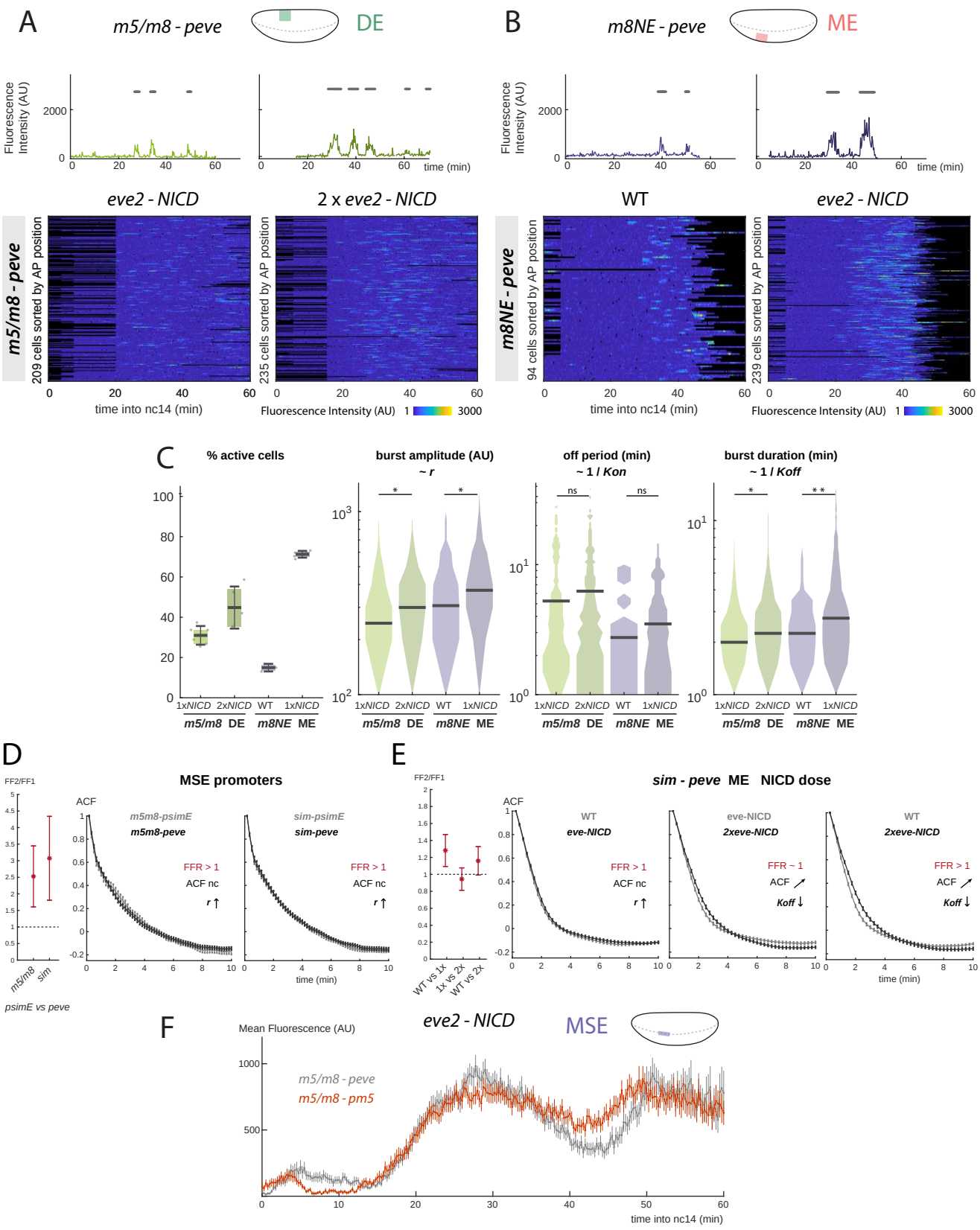

Figure S4. Effects of NICD on the transcriptional bursting properties. A) Example traces and heatmaps of cells showing bursts of transcriptional activity from *m5/m8* in the dorsal ectoderm region in conditions of ectopic Notch activity. **B**) Example traces and heatmaps of cells showing bursts of transcriptional activity from *m8NE* in the mesoderm in wild type and *eve2-NICD* embryos. Burst periods are marked with a grey line. **C**) Quantification of the effects of NICD

Figure S4 (continued). levels on the bursting properties. In both enhancers higher NICD produces a greater proportion of active cells and bigger bursts (increased amplitude and duration). **D**-**E**) Plots showing the Fano factor ratio and changes ACF over time (FFRatio in red, ACF in grey/black plots). FFRatio plots mean and SD of the FFRatio (FF2/FF1) in 50 bootstraps. Dashed line indicates 1 to compare the obtained FFRatio values. ACF plots compare mean and SD of the ACF of all available MS2 traces in 50 bootstraps from two conditions (grey and black lines as indicated, the mean levels are always higher in the condition plotted with a black line). **D**) Analysis of traces from reporters containing different promoters reveals changes in the mean are due to changes in r (FFRatio greater than 1 and no changes in the ACF). **E**) Comparison of the FF ratio and ACF in ME traces from *sim* in WT, *eve2-NICD* and 2x*eve2-NICD* reveals changes in the mean are consistent with increases in r (WT vs *eve2-NICD* comparison, left) or decreases in K_{off} (middle and right plots comparing *eve2-NICD* vs 2x*eve2-NICD* and WT vs *eve2-NICD*; ACF shifts to the right from the lower to higher mean condition). Note that the model assumes only one parameter changes. **F**) Higher NICD levels saturate the response from the effect on the enhancer. A promoter that produces higher mean levels in wild type embryos does not increase the levels with *eve2-NICD*. Differential distributions in **C** tested with two-sample Kolmogorov-Smirnov test: pvalues <0.01(*), $<10^{-5}$(**), $<10^{-10}$(***). n = 6 (*m5/m8 eve2-NICD* lateral view), 5 (*m5/m8* 2x*eve2-NICD* lateral view), 3 (*m8NE* WT), 5 (*m8NE eve2-NICD*) and 5 (*m5/m8-pm5 eve2-NICD*) embryos. Grey lines in **F** are re-plotted from Fig. 3**E**.

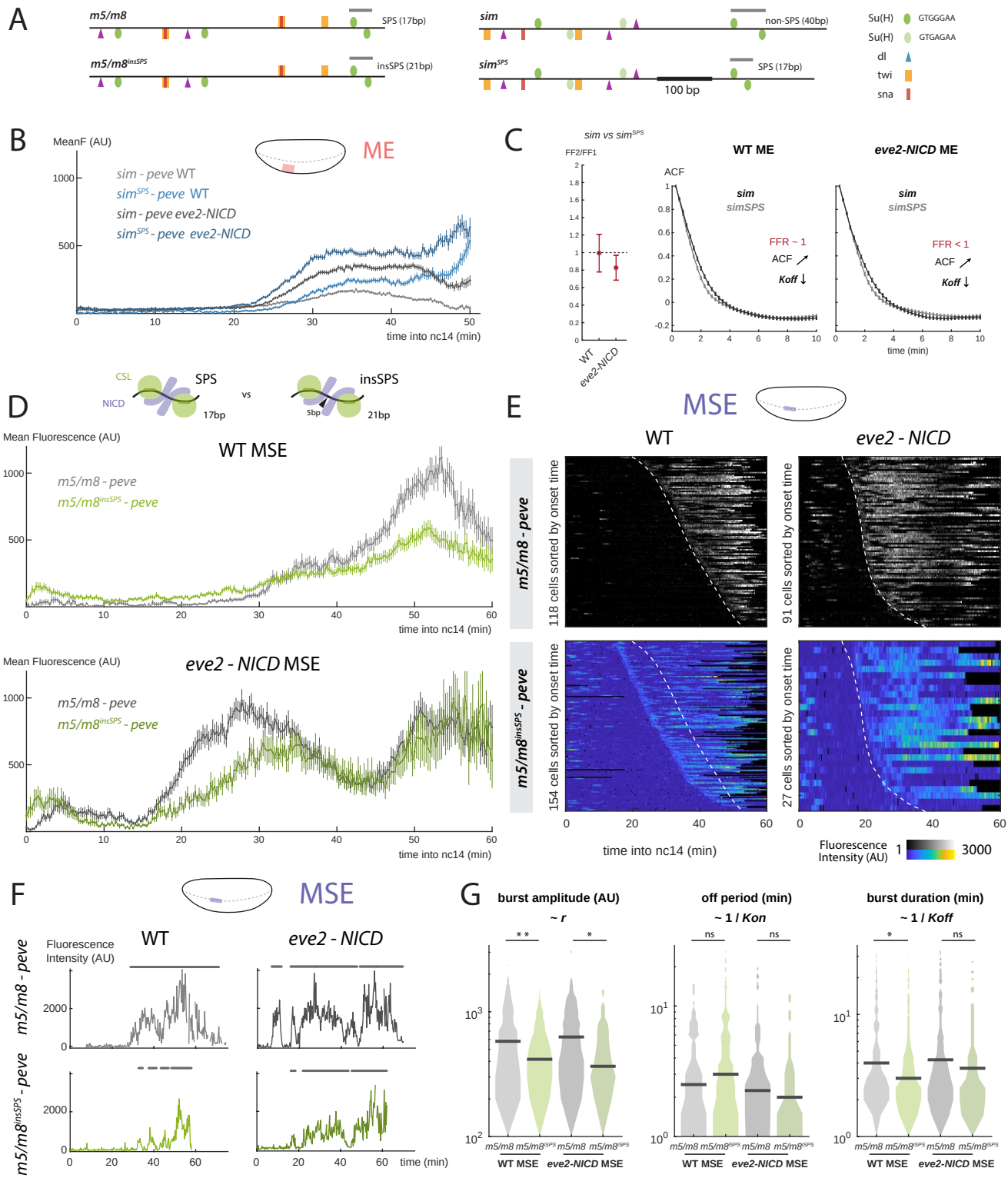

Figure S5. Disruption of a SPS site produces lower transcription levels but does not delay the onset of transcription. **A**) Schematic representation of Su(H), Dorsal, Twist and Snail binding motifs in *m5/m8* and *sim* and introduced alterations in the SPS sites. **B**) sim^{SPS} produces higher mean levels in the mesoderm compared to *sim*, in both wild type and *eve2-NICD* embryos. **C**) Plots showing the Fano factor ratio and changes ACF over time (FFRatio in red, ACF in grey/black plots). The Fano factor ratio and autocorrelation function of *sim* and sim^{SPS} traces in the mesoderm in wild type and *eve2-NICD* embryos are compatible with changes in $Koff$ (shift in ACF) to produce increases in mean levels from *sim* to sim^{SPS}, in agreement with 5**D**. **D**) $m5/m8^{insSPS}$ produces lower mean levels of transcription compared to *m5/m8* but does not delay the onset of the response. **E**) $m5/m8^{ins}$ does not shift the onset of the response in *eve2-NICD*

Figure S5 (continued). embryos (bottom) compared to *m5/m8* but presents some de-repression in wild type embryos (top). Dashed lines indicate onset times in the wild type enhancer. **F**) Examples of fluorescent traces in the mesectoderm region in the described conditions. Burst periods are marked with a grey line. **G**) Quantification of the busting properties in the mesectoderm. $m5/m8^{insSPS}$ produces smaller bursts (lower amplitude and shorter duration) than *m5/m8*. Differential distributions in **G** tested with two-sample Kolmogorov-Smirnov test: pvalues <0.01(*), $<10^{-5}$(**), $<10^{-10}$(***). n = 5 ($m5/m8^{insSPS}$ WT), 3 ($m5/m8^{insSPS}$ *eve2-NICD*). Grey lines and heatmaps in **DE** are re-plotted from Fig. 3**ED**. **C** shows mean and SD over time of the mean Fano factor ratio and mean ACF over 50 bootstraps of all traces.

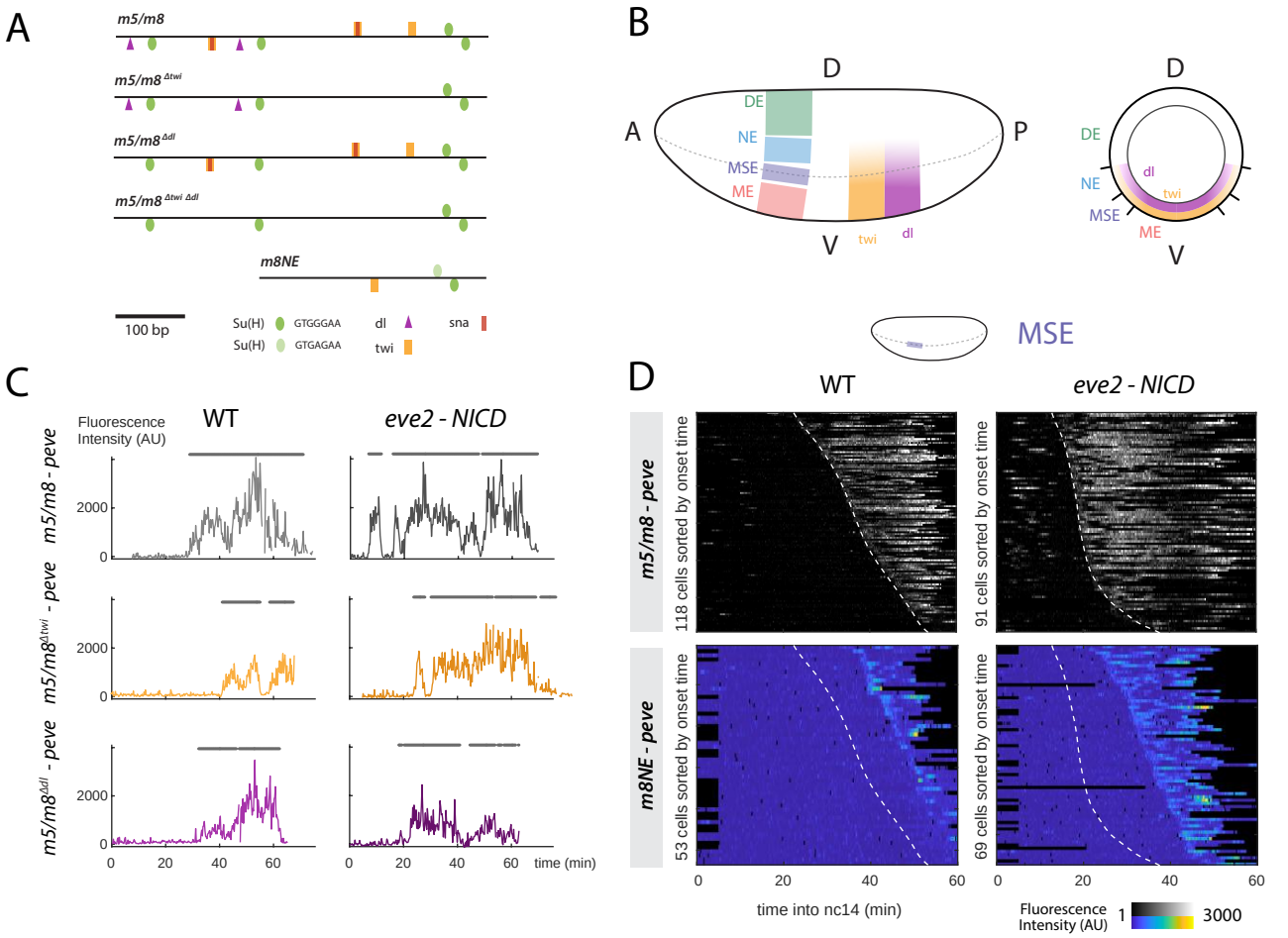

Figure S6. Effects of mutations in Twist or Dorsal motifs in the onset of transcription. **A**) Schematic representation of the introduced mutations in *m5/m8* and comparison with a neuroectodermal enhancer, *m8NE*. **B**) Diagram of Twist and Dorsal gradients in the blastoderm embryo, showing lateral view (left) and cross-section (right). Both gradients extend in a ventral to dorsal gradient in the ME, MSE and NE. **C**) Examples of transcription traces from mesectodermal cells expressing *m5/m8* with mutated Twist or Dorsal motifs. The onset of transcription is delayed but transcription still occurs in a sustained manner. **D**) Heatmaps of MSE cells expressing *m8NE*. The onset of transcription is delayed compared to *m5/m8*. Dashed lines indicate onset times in the *m5/m8*.

Table 1. Primers used to amplify enhancer and promoter sequences and to introduce mutations in the enhancers. Restriction sites for *Hind*III, *Age*I and *Eag*I are underlined.

Primer name	Sequence
m5/m8 S	AAGCTTTGTTCCGTTTGGTAAAACCC
m5/m8 AS	ACCGGTCTTTCCACTGACATTCGAATC
sim S	AAGCTTCCCCGGCATATGTTACGCAC
sim AS	ACCGGTGGTTACAGGCAAACAGCAAAC
m8NE S	AAGCTTGGATCCCCTGCCCCTGCTC
m8NE AS	ACCGGTAACTTCGTAGGACGGAGGAC
peve S	AATGTCAGTGGAAAGACCGGTTTGCCTGCAGAGCGCAGCG
peve AS	TCCAAGGGCGAATTCACCGGCCGAACGAAGGCAGTTAGTTGTTGACTGT
hsp70 S	AATGTCAGTGGAAAGACCGGTGAGCGCCGGAGTATAAATAGA
hsp70 AS	TCCAAGGGCGAATTCACCGGCCGTATTCAGAGTTCTCTTCTTGTATTC
pm5 S	AATGTCAGTGGAAAGACCGGTACGCACGCACAGCATAGCAAT
pm5 AS	TCCAAGGGCGAATTCACCGGCCGAAGATTTGTAGAAATGTGCTGAGCTG
pm6 S	AATGTCAGTGGAAAGACCGGTTGGGATGATGTTGCTGCTG
pm6 AS	TCCAAGGGCGAATTCACCGGCCGTGTAGTATCACTTTACAGATAAGAGT
pm7 S	AATGTCAGTGGAAAGACCGGTAGTTTGCTCCGCAGGTGGT
pm7 AS	TCCAAGGGCGAATTCACCGGCCGATCTTTCGGAGGAGGTTATCCTG
pm8 S	AATGTCAGTGGAAAGACCGGTGCAGCTGTTCCTTGTGAAAAA
pm8 AS	TCCAAGGGCGAATTCACCGGCCGTTTGAAAAATTTTGTATTCGGCT
psimE S	AATGTCAGTGGAAAGACCGGTGTGTGAGTGTGGTGCATATAAATTTCGC
psimE S	TCCAAGGGCGAATTCACCGGCCGGCGCACTCGCCGATGGTTAGTCA
sim for simSPS S	AAGTGTTTCCCACGATTCTGTCCTCCTTATGTGAAACTC
sim for simSPS AS	TCAAGTTTCCCACAAGATGGAAAGTGGAGAGTCCATAA
SPS from m5/m8 S	ATGGACTCTCCACTTTCCATCTTGTGGGAAACTTGAGG
SPS from m5/m8 AS	TTTCACATAAGGAGGACAGAATCGTGGGAAACACTTT
insSPS S	TGAGGGCAAAGAGGGGTGTTTCCCACGATTCGAAT
insSPS AS	TGGGAAACACCCCTCTTTGCCCTCAAGTTTCCCAC
mut Twi 1 S	ACTGATTTCCGTCCCAATGAGTCCCAAAATTGCACACATC
mut Twi 1 AS	TTTGGGACTCATTGGGACGGAAATCAGTATCTTACGGATT
mut Twi 2 S	CAAAATTCCCATTAGGACATCATCGGTTTGGCCCACTGTG
mut Twi 2 AS	AACCGATGATGTCCTAATGGGAATTTTGAGGGTGCCTTGC
mut Twi 3 S	CGGGACTCGCATTCGGACAACCTCCGATTATAACTTATAA
mut Twi 3 AS	ATCGGAGGTTGTCCGAATGCGAGTCCCGAGTCCGAGCTCC
mut dl 1 S	CCGTTTGGTGAGATCTCAAAAATCACATTCGAAAA
mut dl 1 AS	TGATTTTTGAGATCTCACCAAACGGAACAAAGCTT
mut dl 2 S	TCGCCTTGGGAGATCTCATTTCCGACATCCCAAAA
mut dl 2 AS	TCGGAAATGAGATCTCCCAAGGCGAAGATGTGTGC

Supplemental movies

Movie 1. Expression of *m5/m8-peve*. Movie showing transcription from *m5/m8-peve* in broad domains during nuclear cycles 10-13 and in the mesectoderm stripe during nc14. Maximum intensity projection (19x1um stacks) of the MCP-GFP (grey in left pannel, green in right pannel) and His2Av-RFP (blue in right pannel) channels. 0.36 um/px XY resolution and final time resolution of 10s/frame. Anterior to the left; embryo imaged from the ventral side.

Movie 2. Expression of *sim-peve*. Movie showing transcription from *sim-peve* in broad domains during nuclear cycles 10-13 and in the mesectoderm stripe and some mesodermal cells during nc14. Maximum intensity projection (29x1um stacks) of the MCP-GFP (grey in left pannel, green in right pannel) and His2Av-RFP (blue in right

pannel) channels. 0.36 um/px XY resolution and final time resolution of 15s/frame. Anterior to the left; embryo imaged from the ventral side.

Movie 3. Ectopic expression of *m5/m8* with *eve2-NICD*. Movie showing ectopic transcription from *m5/m8-peve* in the *eve2* domain during nc14. Maximum intensity projection (29x1um stacks) of the MCP-GFP (grey in left pannel, green in right pannel) and His2Av-RFP (blue in right pannel) channels. 0.36 um/px XY resolution and final time resolution of 15s/frame. Anterior to the left; embryo imaged from the ventral side.

Movie 4. Ectopic expression of *sim* with *eve2-NICD*. Movie showing ectopic transcription from *sim-peve* in the *eve2* domain during nc14. Maximum intensity projection (29x1um stacks) of the MCP-GFP (grey in left pannel, green in right pannel) and His2Av-RFP (blue in right pannel) channels. 0.36 um/px XY resolution and final time resolution of 15s/frame. Anterior to the left; embryo imaged from the ventral side.

Movie 5. Regions of ectopic expression of *m5/m8* and *sim* with *eve2-NICD*. Combined movie of *m5/m8-peve* (left) and *sim-peve* (right) showing ectopic transcription in the *eve2* stripe. The maximum projection of the MCP-GFP signal is overlayed with tracked nuclei false colored with the maximum intensity pixel in each nuclei. Active nuclei in each of the analyzed regions is marked with a different color: red (mesoderm), purple (mesectoderm), blue (neuroectoderm) and green (dorsal ectoderm). Anterior to the left; embryo imaged from the ventral side.

Modelling changes in kinetic parameters of transcription

We used a two-state promoter model of transcriptional activation in which the promoter switches between OFF and ON with constants K_{on} and K_{off} and releases mRNAs at a rate r when the promoter is ON (Fig.4**E**). This model also accounts for the residence time of polymerase on DNA while transcribing the gene (the elongation time T), so it is capturing what the MS2 system detects, ie. the number of nascent mRNA on the gene, rather than overall levels of mRNA in the cell. We take as a starting point expressions from (Choubey et al. 2015) for the mean and variance of the number of nascent mRNAs (m) in steady state:

$$\langle m \rangle = \frac{rTK_{on}}{K_{on} + K_{off}} \tag{1}$$

$$Var(m) = \langle m \rangle \left[1 + \frac{2rK_{off}}{(K_{on} + K_{off})^2} + \frac{2rK_{off}}{(K_{on} + K_{off})^3} \left(\frac{e^{-T(Kon+Koff)} - 1}{T} \right) \right] \tag{2}$$

We take the elongation time, T, to be fixed for a given gene. Thus, according to equation 1, the levels of transcription could increase in three ways: by increasing r, increasing K_{on}, or decreasing K_{off}.

Thus, because of this degeneracy, observing a change in $\langle m \rangle$ is alone insufficient to determine which underlying bursting parameter is being tuned to drive that change. However, we can make progress by incorporating the

intrinsic noise of transcription into our analysis, since equation 2 indicates that changes to bursting parameters that have equivalent effects on the mean may nonetheless lead to different noise signatures. To do this, we calculate the Fano factor, which is defined as the variance divided by the mean:

$$Fano(m) = \frac{Var(m)}{\langle m \rangle} \tag{3}$$

$$= 1 + \frac{2rK_{off}}{(K_{on} + K_{off})^2} + \frac{2rK_{off}}{(K_{on} + K_{off})^3}\left(\frac{e^{-T(K_{on}+Koff)} - 1}{T}\right) \tag{4}$$

Where we see that the expression for the Fano factor is identical to the quantity inside the brackets in equation 2.

Next, we examine how changes to each bursting parameter in turn will affect the Fano factor and Mean, respectively, demonstrating how these signatures can be used to uncover the drivers of observed changes between different experimental conditions.

Pol II Initiation Rate (r)

We start by considering the case when r is modulated. In the discussions that follow, we assume a situation in which we are comparing two experimental conditions that exhibit observable differences in their mean rate of expression, $\langle m \rangle$:

$$\alpha\langle m_1 \rangle = \langle m_2 \rangle \tag{5}$$

Our goal is to determine whether the modulation of specific parameters corresponds reliably with changes in the mean and Fano factor. To do this, we undertake analysis of the functional form of the partial derivatives of these empirical measures with respect to each parameter.

From equation 1, we have:

$$\frac{\partial\langle m \rangle}{\partial r} = \frac{TK_{on}}{\kappa} \tag{6}$$

$$\frac{\partial\langle m \rangle}{\partial r} > 0 \tag{7}$$

Where, for convenience, we have introduced the shorthand $\kappa = K_{on} + K_{off}$. So we see that $\langle m \rangle$ is monotonic with r: an increase in r always leads to an increase in the mean (and vice versa). The strict inequality applies because

the right-hand-side of eq. 6 can be zeros *if* no expression occurs. For the fano Factor, we have:

$$\frac{\partial Fano}{\partial r} = \frac{2K_{off}}{\kappa^2}\left(1 + \frac{e^{-\kappa T} - 1}{\kappa T}\right) \tag{8}$$

$$\frac{\partial Fano}{\partial r} \geq 0 \tag{9}$$

Unlike the mean, it is possible that a change in r could lead to *no* observable modulation in the Fano factor; however, this only holds for exceptionally small values of κT. More importantly, we see that it is impossible for the Fano factor to decrease when r is increased. Thus, we conclude that an increase in r must coincide with an increase in both the mean rate of expression and in the Fano factor, ie. the ratio between the Fano factors $Fano(m_2)$ and $Fano(m_1)$ where $\langle m_2 \rangle = \alpha \langle m_1 \rangle$ would always be greater than 1 (Fig. S3**D**, top panel).

Activation Rate (K_{on})

As with r, we begin by examining how $\langle m \rangle$ changes in response to a change in K_{on}:

$$\frac{\partial \langle m \rangle}{\partial K_{on}} = \frac{rT}{\kappa} - \frac{rTK_{on}}{\kappa^2} \tag{10}$$

$$= \frac{rT}{\kappa}(1 - \frac{K_{on}}{\kappa}) \tag{11}$$

$$\frac{\partial \langle m \rangle}{\partial K_{on}} \geq 0 \tag{12}$$

Thus, as with r, the mean rate of expression increases monotonically in response to increases in K_{on}. Next, for the Fano factor, we have:

$$\frac{\partial Fano}{\partial k_{on}} = 2rK_{off}\Big(- \kappa^{-3}(2 + e^{-\kappa T}) + \frac{3\kappa^{-4}}{T}(1 - e^{-\kappa T})\Big) \tag{13}$$

$$= -\frac{2rK_{off}}{\kappa^3}\Big(2 + e^{-\kappa T} - \frac{3(1 - e^{-\kappa T})}{\kappa T}\Big) \tag{14}$$

To gain further insight, we need to examine limiting cases for the quantity κT, which encodes the relative magnitude of the elongation time and switching rates, and which dictates the noise characteristics of the system.

We start with the case where $\kappa T << 1$:

$$\frac{\partial Fano}{\partial k_{on}} \approx -\frac{2rK_{off}}{\kappa^3}\Big(2+1-\kappa T-\frac{3(1+\kappa T-1)}{\kappa T}\Big) \tag{15}$$

$$\approx -\frac{2rK_{off}}{\kappa^3}\Big(3-\kappa T-3\Big) \tag{16}$$

$$\approx -\frac{2rK_{off}}{\kappa^3}(0) \tag{17}$$

$$\approx -\frac{2rK_{off}}{\kappa^3}\Big(3-\kappa T-3\Big) \tag{18}$$

$$\frac{\partial Fano}{\partial k_{on}} \approx 0 \tag{19}$$

For the opposite limit, where $\kappa T >> 1$, we have:

$$\frac{\partial Fano}{\partial k_{on}} \approx -\frac{2rK_{off}}{\kappa^3}\Big(2+0-\frac{3(1-0)}{\kappa T}\Big) \tag{20}$$

$$\approx -\frac{4rK_{off}}{\kappa^3} \tag{21}$$

$$\frac{\partial Fano}{\partial k_{on}} \leq 0 \tag{22}$$

So we see that, an increase in $\langle m \rangle$ that is driven by an increase in K_{on} will coincide with a *decrease* in the Fano factor. Thus, unlike r, where the signs of the change in the mean and Fano factor are the same, we find that the signs of the changes in the mean and Fano factor are opposite in the case of changes driven by K_{on}, ie. the ratio between the Fano factors $Fano(m_2)$ and $Fano(m_1)$ where $\langle m_2 \rangle = \alpha \langle m_1 \rangle$ would always be smaller than 1 (Fig. S3**D**, middle panel).

Off Rate (K_{off})

For the mean, we have:

$$\frac{\partial \langle m \rangle}{\partial K_{off}} = -\frac{rK_{on}}{\kappa^2} \tag{23}$$

$$\frac{\partial \langle m \rangle}{\partial K_{off}} \leq 0 \tag{24}$$

Thus, as expected, an increase in K_{off} leads to a *decrease* in $\langle m \rangle$. In keeping with our treatment in the case of K_{on}, we next examine the functional form of the Fano factor in the small and large κT limits. For $\kappa T << 1$, we

expand about $\kappa T = 0$ to obtain an expression for the Fano factor :

$$Fano \approx 1 + \frac{2rK_{off}}{(K_{on}+K_{off})^2} + \frac{2rK_{off}}{(K_{on}+K_{off})^3}\left(\frac{1-\kappa T-1}{T}\right) \tag{25}$$

$$\approx 1 \tag{26}$$

Thus, consistent with our findings for K_{on} the Fano Factor is largely insensitive to changes in K_{off} for small κT. This holds for r as well, though we did not state so explicitly above. Next, we approximate the large κT limit by setting $e^{-kT} = 0$:

$$Fano \approx 1 + \frac{2rK_{off}}{\kappa^2} + \frac{2rK_{off}}{\kappa^3}\left(\frac{0-1}{T}\right) \tag{27}$$

$$\approx 1 + 2r\left(\frac{K_{off}}{\kappa^2} - \frac{K_{off}}{\kappa^2}\frac{1}{\kappa T}\right) \tag{28}$$

$$\approx 1 + 2r\left(\frac{K_{off}}{\kappa^2}\right) \tag{29}$$

Differentiating, we obtain:

$$\frac{\partial Fano}{\partial_{off}} \approx 2r\left(\frac{1}{\kappa^2} - \frac{2K_{off}}{\kappa^3}\right) \tag{30}$$

$$\approx \frac{2r}{\kappa^2}\left(1 - \frac{2K_{off}}{\kappa}\right) \tag{31}$$

The expression above reveals that, unlike r and K_{on}, the direction of the change of the Fano Factor in response to a change in K_{off} not fixed, but depends upon the relative sizes of K_{on} and K_{off}, ie. the ratio between the Fano factors $Fano(m_2)$ and $Fano(m_1)$ where $\langle m_2 \rangle = \alpha \langle m_1 \rangle$ could be smaller or greater than 1 (Fig.S3**D**, bottom panel). Numerical simulations confirm this result.

Stochastic simulations

We next tested with simulations whether the Fano factor ratio can be used as a diagnostic tool of the underlying changes in the mean. We used stochastic simulations of transcription based on the Gillespie algorithm (Gillespie 1976) of the same two-state promoter model but using additional parameters to more resemble the biological MS2 data (accounting for the time MS2 loops are detected, acquisition time and adding experimental noise, Fig. S3**F**).

We then tested whether we could recover the same trends in Fano factor ratios in the simulation as expected from the mathematical model. Indeed, using a variety of starting parameters we could recover similar Fano factor

values as expected from the mathematical model (Fig. S3**D**). However, given that changes in K_{off} can produce Fano factor ratios greater or smaller than 1, calculation of the Fano factor and comparing whether it is greater or smaller than 1 alone is not sufficient to infer which parameter is being modified to produce the observed changes in the mean.

Utilizing the Autocorrelation Function (ACF)

The results of our analysis thus far indicate that modulations in r and K_{on} lead to distinct, well defined signatures in mean and Fano factors of experimentally observed expression levels. However, the degeneracy of the Fano factor shift with respect to changes in K_{off} necessitates the incorporation of an additional observable, if we are to be able to distinguish the underlying drivers of changes between experimental conditions. To this end, we utilize the empirical Autocorrelation Function of our experimental MS2 traces.

The ACF function provides information about the speed of the system and the elongation rate (Desponds et al. 2016; Lammers et al. 2018). Intuitively, the more rapid the time scale with which the system switches between activity states (the larger κ is), the faster the ACF decays. We used the same simulations to test if the autocorrelation function changes in different ways depending on the modified parameters, to help distinguishing between the 3 scenarios to increase the mean. If the dynamics are fast (Fig.S3**E**, right column, $K_{on1} = 0.1s^{-1}$ and $K_{on1} = 0.2s^{-1}$) no changes in the ACF were observed in any of the three cases. When the dynamics are slower (Fig.S3**E**, left column, $K_{on1} = 0.01s^{-1}$ and $K_{on1} = 0.02s^{-1}$), then the AC function shifts to the right (from $\langle m_1 \rangle$ to $\langle m_2 \rangle$) when K_{off} decreases. No changes are observed when r or K_{on} increase.

Therefore looking at both the Fano factor ratio and the autocorrelation function (when the dynamics are slow enough), provides enough information to distinguish between the three ways in which the mean can change (Fig. S3**B**):

- increase in r: FFRatio > 1 and no change in ACF
- increase in K_{on}: FFRatio < 1 and no change in ACF
- decrease in K_{off}: FFRatio < 1 or > 1 and shift to the right in ACF

Estimating Fano factor from empirical data

When applied to real MS2 traces, raw fluorescence profiles from each cell were processed by applying a median filter of 3, removing the background baseline and normalizing for bleaching as described in the Methods section. When the onset of transcription was different between experiments (eg. WT vs *eve2-NICD*) they were

shifted to compare equivalent times. The Fano factor was calculated as the intrinsic variability divided by the mean over time:

$$Fano = \frac{\sigma_i^2}{\langle m \rangle} \tag{32}$$

$$= \frac{Var(m) - CoVar(m)}{\langle m \rangle} \tag{33}$$

The intrinsic component was calculated by subtracting an estimation of the extrinsic variability form the total noise. The contribution from the extrinsic noise, normally calculated from the covariance of two transcription traces from the same cell, was calculated by using neighbouring nuclei as proxi of two loci in the same cell and calculating their covariance. Using the experiments where two MS2 reporters are present in each cell we validated the contribution from extrinsic noise is equivalent within cell and across neighbouring cells. Both FFRatio and ACF were calculated by doing 50 bootstraps of all available traces and calculating the mean and SD.

The code used to simulate MS2 traces and calculate the Fano factor and ACF is available at GitHub:FFR_ACF.

Acknowledgments

We thank members of the Bray Lab and of the Notch community for helpful discussions and Bill Harris and Maria J. Gomez-Lamarca for comments on the manuscript. Thanks to the Sanson, Small and St Johnston, labs for providing flies and plasmids and to Kat Millen and the Genetics Fly Facility for injections. This work was supported by a Programme grant from the Medical Research Council to SJB and by a PhD studentship to JFS from the Wellcome Trust (109144/Z/15/Z). HGG was supported by the Burroughs Wellcome Fund Career Award at the Scientific Interface, the Sloan Research Foundation, the Human Frontiers Science Program, the Searle Scholars Program, the Shurl & Kay Curci Foundation, the Hellman Foundation, the NIH Director's New Innovator Award (DP2 OD024541-01), and an NSF CAREER Award (1652236). NL was supported by NIH Genomics and Computational Biology training grant 5T32HG000047-18. We also want to thank the Physical Biology of the Cell Course at the Marine Biological Laboratory (Woods Hole, MA), where the modelling approached used in this work developed.

The authors declare no competing interests

Author contributions: JFS and SJB planned the experiments; JFS conducted the experiments; JFS,NL,HG developed the computational modelling and analysis; JFS, SJB wrote the manuscript; NL,HG edited the manuscript.

References

Bailey, A.M. and Posakony, J.W. (1995). Suppressor of hairless directly activates transcription of enhancer of split complex genes in response to Notch receptor activity. Genes Dev. *9*.21, 2609–2622.

Bartman, C.R., Hsu, S.C., Hsiung, C.C.-S., Raj, A., and Blobel, G.A. (2016). Enhancer Regulation of Transcriptional Bursting Parameters Revealed by Forced Chromatin Looping. Mol. Cell *62*.2, 237–247.

Berrocal, A., Lammers, N.C., Garcia, H.G., and Eisen, M.B. (2018). Kinetic sculpting of the seven stripes of the Drosophila even-skipped gene. bioRxiv, 335901.

Bischof, J., Maeda, R.K., Hediger, M., Karch, F., and Basler, K. (2007). An optimized transgenesis system for Drosophila using germ-line-specific phiC31 integrases. Proc. Natl. Acad. Sci. U. S. A. *104*.9, 3312–7.

Bischof, J. et al. (2013). A versatile platform for creating a comprehensive UAS-ORFeome library in Drosophila. Development *140*.11, 2434–42.

Blackwood, E.M. and Kadonaga, J.T. (1998). Going the distance: A current view of enhancer action. Science (80-.). *281*.5373, 60–63.

Boija, A. et al. (2018). Transcription Factors Activate Genes through the Phase-Separation Capacity of Their Activation Domains. Cell, 1–14.

Boije, H., Rulands, S., Dudczig, S., Simons, B.D., and Harris, W.A. (2015). The Independent Probabilistic Firing of Transcription Factors: A Paradigm for Clonal Variability in the Zebrafish Retina. Dev. Cell *34*.5, 532–543.

Bothma, J.P., Garcia, H.G., Esposito, E., Schlissel, G., Gregor, T., and Levine, M. (2014). Dynamic regulation of eve stripe 2 expression reveals transcriptional bursts in living Drosophila embryos. Proc. Natl. Acad. Sci. *111*.29, 10598–10603.

Bothma, J.P., Norstad, M.R., Alamos, S., and Garcia, H.G. (2018). LlamaTags: A Versatile Tool to Image Transcription Factor Dynamics in Live Embryos. Cell *173*.7, 1810–1822.e16.

Bray, S.J. (2006). Notch signalling: A simple pathway becomes complex. Nat. Rev. Mol. Cell Biol. *7*.9, 678–689.

Chang, H.H., Hemberg, M., Barahona, M., Ingber, D.E., and Huang, S. (2008). Transcriptome-wide noise controls lineage choice in mammalian progenitor cells. Nature *453*.7194, 544–547.

Chen, H., Levo, M., Barinov, L., Fujioka, M., Jaynes, J.B., and Gregor, T. (2018). Dynamic interplay between enhancer–promoter topology and gene activity. Nat. Genet. *50*.9, 1296–1303.

Cho, W.K., Spille, J.H., Hecht, M., Lee, C., Li, C., Grube, V., and Cisse, I.I. (2018). Mediator and RNA polymerase II clusters associate in transcription-dependent condensates. Science (80-.). *361*.6400, 412–415.

Cho, W.K. et al. (2016). RNA Polymerase II cluster dynamics predict mRNA output in living cells. Elife *5*.MAY2016, 1–31.

Choubey, S., Kondev, J., and Sanchez, A. (2015). Deciphering Transcriptional Dynamics In Vivo by Counting Nascent RNA Molecules. PLoS Comput. Biol. *11*.11, 1–21. arXiv: 1311.0050.

Chubb, J.R., Trcek, T., Shenoy, S.M., and Singer, R.H. (2006). Transcriptional Pulsing of a Developmental Gene. Curr. Biol. *16*.10, 1018–1025.

Cowden, J. and Levine, M. (2002). The Snail repressor positions Notch signaling in the Drosophila embryo. Development *129*.7, 1785–93.

De Renzis, S., Yu, J., Zinzen, R., and Wieschaus, E. (2006). Dorsal-ventral pattern of Delta trafficking is established by a snail-tom-neuralized pathway. Dev. Cell *10*.2, 257–264.

Desponds, J., Tran, H., Ferraro, T., Lucas, T., Perez Romero, C., Guillou, A., Fradin, C., Coppey, M., Dostatni, N., and Walczak, A.M. (2016). Precision of Readout at the hunchback Gene: Analyzing Short Transcription Time Traces in Living Fly Embryos. PLOS Comput. Biol. *12*.12, e1005256.

Elowitz, M.B. (2002). Stochastic Gene Expression in a Single Cell. Science (80-.). *297*.5584, 1183–1186.

Fritzsch, C., Baumgärtner, S., Kuban, M., Steinshorn, D., Reid, G., and Legewie, S. (2018). Estrogen-dependent control and cell-to-cell variability of transcriptional bursting. Mol. Syst. Biol. *14*.2, e7678.

Fukaya, T., Lim, B., and Levine, M. (2016). Enhancer Control of Transcriptional Bursting. Cell *166*.2, 358–368.

Garcia, H.G., Tikhonov, M., Lin, A., and Gregor, T. (2013). Quantitative Imaging of Transcription in Living Drosophila Embryos Links Polymerase Activity to Patterning. Curr. Biol. *23*.21, 2140–2145.

Gibson, D.G. (2011). "Enzymatic Assembly of Overlapping DNA Fragments". Vol. 498, pp. 349–361.

Gillespie, D.T. (1976). A general method for numerically simulating the stochastic time evolution of coupled chemical reactions. J. Comput. Phys. *22*.4, 403–434.

Golding, I., Paulsson, J., Zawilski, S.M., and Cox, E.C. (2005). Real-time kinetics of gene activity in individual bacteria. Cell *123*.6, 1025–1036.

Gomez-Lamarca, M.J. et al. (2018). Activation of the Notch Signaling Pathway In Vivo Elicits Changes in CSL Nuclear Dynamics. Dev. Cell *44*.5, 611–623.e7.

Harper, C.V. et al. (2011). Dynamic analysis of stochastic transcription cycles. PLoS Biol. *9*.4.

Kopczynski, C.C., Alton, A.K., Fechtel, K., Kooh, P.J., and Muskavitch, M.A. (1988). Delta, a Drosophila neurogenic gene, is transcriptionally complex and encodes a protein related to blood coagulation factors and epidermal growth factor of vertebrates. Genes Dev. *2*.12 B, 1723–1735.

Kosman, D. and Small, S. (1997). Concentration-dependent patterning by an ectopic expression domain of the Drosophila gap gene knirps. Development *124*.7, 1343–1354.

Kramatschek, B. and Campos-Ortega, J.a. (1994). Neuroectodermal transcription of the Drosophila neurogenic genes E(spl) and HLH-m5 is regulated by proneural genes. Development *120*.4, 815–826.

Lammers, N.C., Galstyan, V., Reimer, A., Medin, S.A., Wiggins, C.H., and Garcia, H.G. (2018). Binary transcriptional control of pattern formation in development. bioRxiv, 335919.

Larson, D.R., Fritzsch, C., Sun, L., Meng, X., Lawrence, D.S., and Singer, R.H. (2013). Direct observation of frequency modulated transcription in single cells using light activation. Elife *2013*.2, 1–20.

Larson, D.R., Singer, R.H., and Zenklusen, D. (2009). A single molecule view of gene expression. Trends Cell Biol. *19*.11, 630–637.

Lee, C., Shin, H., and Kimble, J. (2018). Dynamics of Notch-dependent transcriptional bursting in its native context. submitted.

Lim, B., Heist, T., Levine, M., and Fukaya, T. (2018). Visualization of Transvection in Living Drosophila Embryos. Mol. Cell *70*.2, 287–296.e6.

Little, S.C., Tikhonov, M., and Gregor, T. (2013). Precise developmental gene expression arises from globally stochastic transcriptional activity. Cell *154*.4, 789–800.

Lu, H., Yu, D., Hansen, A.S., Ganguly, S., Liu, R., Heckert, A., Darzacq, X., and Zhou, Q. (2018). Phase-separation mechanism for C-terminal hyperphosphorylation of RNA polymerase II. Nature *558*.7709, 318–323.

Mir, M., Reimer, A., Haines, J.E., Li, X.Y., Stadler, M., Garcia, H., Eisen, M.B., and Darzacq, X. (2017). Dense bicoid hubs accentuate binding along the morphogen gradient. Genes Dev. *31*.17, 1784–1794.

Mishchenko, Y. (2015). A fast algorithm for computation of discrete Euclidean distance transform in three or more dimensions on vector processing architectures. Signal, Image Video Process. *9*.1, 19–27.

Morel, V., Le Borgne, R., and Schweisguth, F. (2003). Snail is required for Delta endocytosis and Notch-dependent activation of single-minded expression. Dev. Genes Evol. *213*.2, 65–72.

Morel, V. and Schweisguth, F. (2000). Repression by Suppressor of Hairless and activation by Notch are required to define a single row of single-minded expressing cells in the Drosophila embryo. Genes Dev. *14*.3, 377–388.

Nam, Y., Sliz, P., Pear, W.S., Aster, J.C., and Blacklow, S.C. (2007). Cooperative assembly of higher-order Notch complexes functions as a switch to induce transcription. Proc. Natl. Acad. Sci. U. S. A. *104*.7, 2103–8.

Nandagopal, N., Santat, L.A., LeBon, L., Sprinzak, D., Bronner, M.E., and Elowitz, M.B. (2018). Dynamic Ligand Discrimination in the Notch Signaling Pathway. Cell *172*.4, 869–880.e19.

Ng, K.K., Yui, M.A., Mehta, A., Siu, S., Irwin, B., Pease, S., Hirose, S., Elowitz, M.B., Rothenberg, E.V., and Kueh, H.Y. (2018). A stochastic epigenetic switch controls the dynamics of T-cell lineage commitment. Elife *7*, 1–38.

Padovan-Merhar, O., Nair, G.P., Biaesch, A.G., Mayer, A., Scarfone, S., Foley, S.W., Wu, A.R., Churchman, L.S., Singh, A., and Raj, A. (2015). Single Mammalian Cells Compensate for Differences in Cellular Volume and DNA Copy Number through Independent Global Transcriptional Mechanisms. Mol. Cell *58*.2, 339–352.

Peccoud, J. and Ycart, B. (1995). Markovian Modeling of Gene-Product Synthesis. Theor. Popul. Biol. *48*.2, 222–234.

Raj, A. and Oudenaarden, A. van (2008). Nature, Nurture, or Chance: Stochastic Gene Expression and Its Consequences. Cell *135*.2, 216–226.

Raser, J.M. and Shea, E.K.O. (2006). Control of Stochasticity in Eukaryotic Gene Expression Jonathan. Science (80-.). *304*.5678, 1811–1814.

Sabari, B.R. et al. (2018). Coactivator condensation at super-enhancers links phase separation and gene control. Science (80-.). *361*.6400, eaar3958.

Senecal, A., Munsky, B., Proux, F., Ly, N., Braye, F.E., Zimmer, C., Mueller, F., and Darzacq, X. (2014). Transcription factors modulate c-Fos transcriptional bursts. Cell Rep. *8*.1, 75–83.

So, L.H., Ghosh, A., Zong, C., Sepúlveda, L.A., Segev, R., and Golding, I. (2011). General properties of transcriptional time series in Escherichia coli. Nat. Genet. *43*.6, 554–560.

Tantale, K. et al. (2016). A single-molecule view of transcription reveals convoys of RNA polymerases and multi-scale bursting. Nat. Commun. *7*.

Tsai, A., Muthusamy, A.K., Alves, M.R., Lavis, L.D., Singer, R.H., Stern, D.L., and Crocker, J. (2017). Nuclear microenvironments modulate transcription from low-affinity enhancers. Elife *6*.2, 158–160.

Vässin, H. and Campos-Ortega, J.A. (1987). Genetic Analysis of Delta, a Neurogenic Gene of Drosophila melanogaster. Genetics *116*.3, 433–45.

Wernet, M.F., Mazzoni, E.O., Celik, A., Duncan, D.M., Duncan, I., and Desplan, C. (2006). Stochastic spineless expression creates the retinal mosaic for colour vision. Nature *440*.7081, 174–180.

Xu, H., Sepúlveda, L.A., Figard, L., Sokac, A.M., and Golding, I. (2015). Combining protein and mRNA quantification to decipher transcriptional regulation. Nat. Methods *12*.8, 739–742.

Zabidi, M.a., Arnold, C.D., Schernhuber, K., Pagani, M., Rath, M., Frank, O., and Stark, A. (2014). Enhancer-core-promoter specificity separates developmental and housekeeping gene regulation. Nature *518*.7540, 556–559.

Zinzen, R.P., Cande, J., Ronshaugen, M., Papatsenko, D., and Levine, M. (2006a). Evolution of the Ventral Midline in Insect Embryos. Dev. Cell *11*.6, 895–902.

Zinzen, R.P., Senger, K., Levine, M., and Papatsenko, D. (2006b). Computational Models for Neurogenic Gene Expression in the Drosophila Embryo. Curr. Biol. *16*.13, 1358–1365.